

1 **Niclosamide targets macrophages to rescue the disrupted peritoneal homeostasis**
2 **in endometriosis**

3

4 Liang Zhao¹, Mingxin Shi¹, Sarayut Winuthayanon¹, James A. MacLean II¹, Kanako
5 Hayashi^{1,2}

6

7 ¹School of Molecular Biosciences, Center for Reproductive Biology, Washington
8 State University, Pullman, Washington 99164, USA

9

10 ²Correspondence to Kanako Hayashi: k.hayashi@wsu.edu

11

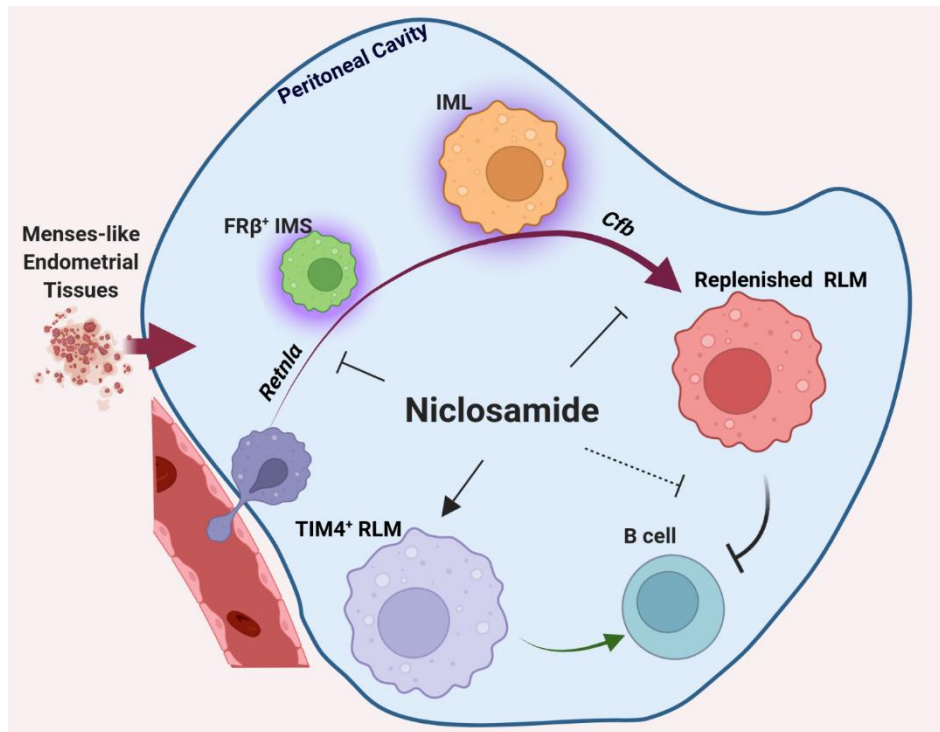
12 Disclosures: The authors declare no competing interests exist.

13

14 Short title: Niclosamide as a new promising therapy for endometriosis

15

16 Summary: Niclosamide tunes the dynamic progression of peritoneal macrophages and
17 their intercellular communications with B cells to rescue the disrupted
18 microenvironment in the peritoneal cavity in a mouse model of endometriosis.



19

20

Graphic Abstract

21 **Abstract**

22 Due to the vital roles of macrophages in the pathogenesis of endometriosis, targeting
23 macrophages could be a new therapeutic direction. Here, we investigated the efficacy
24 of niclosamide for the resolution of perturbed microenvironment caused by
25 dysregulated macrophages in a mouse model of endometriosis. Single-cell
26 transcriptomic analysis revealed the heterogeneity of macrophage subpopulations
27 including three newly identified intermediate subtypes with sharing characteristics of
28 traditional “small” or “large” peritoneal macrophages (SPMs and LPMs) in the
29 peritoneal cavity. Endometriosis-like lesions (ELL) enhanced the differentiation of
30 recruited macrophages, promoted the replenishment of resident LPMs, and increased
31 ablation of embryo-derived LPMs, which were stepwise suppressed by niclosamide.
32 In addition, niclosamide reversed intercellular communications between macrophages
33 and B cells which were disrupted by ELL. Therefore, niclosamide rescued the
34 perturbed microenvironment in endometriosis through its fine regulations on the
35 dynamic progression of macrophages and could be a new promising therapy for
36 endometriosis.

37

38 **Keywords:** niclosamide, endometriosis, macrophages, scRNA-seq, intercellular
39 communications

40 **Introduction**

41 Endometriosis is a common chronic inflammatory disease that affects roughly 10% of
42 reproductive-aged and adolescent women worldwide (Zondervan et al., 2018;
43 Zondervan et al., 2020). It is characterized by the presence and growth of tissues
44 resembling endometrium, termed endometriotic lesions, outside of the uterus. Patients
45 with endometriosis exhibit symptoms of chronic pelvic pain, infertility, and multiple
46 other health issues leading to tremendous reductions in their quality of life
47 (Zondervan et al., 2020). Unfortunately, public and professional awareness of this
48 disease remains poor. Current hormonal therapies, along with laparoscopic surgery,
49 do not cure the disease and are often of limited efficacy with high recurrence rates,
50 frequent side effects, and potential morbidity. Thus, a critical need exists to develop
51 new and effective therapies for endometriosis targeting biologically important
52 mechanisms that underlie the pathophysiology of this disease.

53 Disruption of the immune homeostasis in the peritoneal cavity drives the disease
54 development of endometriosis, and macrophages play a central role in this process
55 (Capobianco and Rovere Querini, 2013; Hogg et al., 2020; Shi et al., 2021).

56 Peritoneal macrophages infiltrate endometriotic lesions and promote their growth and
57 vascularization by releasing proinflammatory cytokines and growth factors (Bacci et
58 al., 2009; Cheong et al., 2002; Sekiguchi et al., 2019; Shi et al., 2021). In addition,
59 IGF1 and netrin-1, along with cytokines secreted by macrophages, also promote
60 neurogenesis and innervation at lesion sites, which enhances the pain sensation in
61 patients (Ding et al., 2021; Forster et al., 2019; Greaves et al., 2015; Scholl et al.,
62 2009). The proinflammatory cytokines released by macrophages disrupted in
63 endometriosis also affect multiple important activities of reproduction, such as
64 hormonal balances and decidualization, leading to infertility (De Ziegler et al., 2010;

65 Rasheed and Hamid, 2020). Suppressing the release of proinflammatory cytokines
66 and growth factors from macrophages inhibits lesion growth and endometriosis-
67 associated pain in rodent models (Bacci et al., 2009; Forster et al., 2019; Liu et al.,
68 2018; Shi et al., 2021). Therefore, targeting peritoneal macrophages that are critical
69 for maintaining immune homeostasis in the pelvic cavity could be a new direction for
70 drug development in endometriosis therapy.

71 To fully characterize the role of peritoneal macrophages in the pathophysiology
72 of endometriosis, a better understanding of the heterogeneity of macrophage
73 populations and their subtype-specific contributions to endometriosis is necessary.
74 Two subsets of macrophages have previously been characterized in the peritoneal
75 cavity and are referred to as “small” (SPMs) and “large” peritoneal macrophages
76 (LPMs) based on both their sizes and frequency (Ghosn et al., 2010). MHC II^{high}
77 F4/80^{low} SPMs are short-lived and are recruited from Ly6C+ classical monocytes,
78 while MHC II^{low} F4/80^{high} LPMs are resident and long-lived with an embryonic origin
79 (Bain et al., 2016; Kim et al., 2016). The population of embryo-derived resident
80 LPMs (RLMs) uniquely express TIM4, and its number is mainly maintained through
81 its self-renewal under physiological conditions (Rosas et al., 2014). With mild
82 inflammation, some of the recruited SPMs gradually differentiate into F4/80^{high}
83 macrophages but still remain in an immature state due to the existence of RLMs (Bain
84 et al., 2016). When the population of RLMs is ablated with extended inflammation,
85 these transitory F4/80^{high} macrophages finally mature and replenish the pool of RLMs
86 (Bain et al., 2016; Liu et al., 2019). However, this newly recruited resident population
87 shows striking functional differences from those embryo-derived ones and thus
88 increasing the risks for the incidence and severity of diseases in the future (Bain et al.,
89 2016). In endometriosis, dynamic and progressive alterations of peritoneal

90 macrophages were also found associated with lesion development (Hogg et al., 2021;
91 Johan et al., 2019). However, the transcriptomic characteristics of peritoneal
92 macrophages especially those transitory subtypes and the molecular signaling
93 networks that coordinate the dynamic progression of macrophages in endometriosis
94 are unknown.

95 Niclosamide is an FDA-approved anthelmintic drug with multiple clinical trials
96 ongoing to repurpose it for the treatment of other diseases including cancer and
97 metabolic diseases (Chen et al., 2018). We previously reported that niclosamide
98 reduced lesion growth, alleviated aberrant inflammation in peritoneal fluids, and
99 decreased the vascularization and innervation in lesions using mouse models of
100 endometriosis (Prather et al., 2016; Shi et al., 2021).

101 In this study, we further focused on the heterogeneity of peritoneal macrophages
102 and molecular mechanisms regulating their dynamic progression after lesion
103 induction using a mouse model of endometriosis. Moreover, we found that
104 niclosamide finely reversed those transcriptomic changes of macrophages caused by
105 lesion induction through its stepwise regulations on the differentiation of recruited
106 macrophages, the maturation of transitory LPMs, and the preservation of embryo-
107 derived RLMs. Niclosamide also rescued the communications between LPMs and B
108 cells which were disrupted by lesion induction. Therefore, we propose that
109 macrophages could be the direct target of niclosamide, and niclosamide could be a
110 new promising therapy for the treatment of endometriosis. Finally, to share our
111 scRNA data with other researchers, we have created a cloud-based web tool
112 (Webpage: <https://kanakohayashilab.org/hayashi/en/mouse/peritoneal.immune.cells/>)
113 for the gene of interest searches that can be easily conducted without the requirement
114 of complicated computer programming skills.

115

116 **Results**

117 **Single-cell transcriptomic sequencing of peritoneal immune cells**

118 In this study, endometriosis-like lesions (ELL) were induced by inoculating mense-
119 like tissues from donor mice into the peritoneal cavity of the recipient, as described in
120 the Method section. Three weeks later, one group of mice was administrated
121 niclosamide (ELL_N) while the others (sham and ELL) were given a control vehicle
122 (Fig. 1A). After another three weeks of treatment, cells in the peritoneal cavity,
123 mostly immune cells, were collected and processed for single-cell transcriptomic
124 analysis. A total of 13,679 cells with a median of 3,160 genes per cell were retained
125 for downstream analysis after quality control and removal of low-quality cells.

126 Integrated cells from all three groups of samples were classified into 19 clusters
127 based on the unsupervised clustering workflow of the Seurat package with cell
128 identities determined by canonical marker gene distributions (Fig. 1B and S1A). Cells
129 from each group showed a consistent distribution of each cluster in UMAP (Fig.
130 S1B), suggesting an unbiased capture of cell populations between groups of different
131 treatments. Macrophages (43%) and B cells (46%) are the most abundant populations
132 identified in peritoneal fluids along with much fewer T cells and other immune cells
133 (Fig. 1B and C).

134

135 **Heterogeneity of peritoneal macrophage populations**

136 Interestingly, 7 sub-clusters of macrophage-related populations (DC1, SPMs, IMS,
137 IML1, IML2, RLMs, and PMs) were identified in these samples (Fig. 1B and C).
138 Clusters of dendritic cells 1 (DC1) and “small” peritoneal macrophages (SPMs)
139 express high levels of characteristic SPMs markers including *H2-Aa* and *Irf4* and are

140 distinguished by the expression of *Cd209a* in DC1 and *Cd226* in SPMs (Fig. 1D and
141 S1C). The identity of resident “large” peritoneal macrophages (RLMs) was
142 determined by the expression of its unique marker, *Timd4* (encodes TIM4, Fig. 1D).
143 In addition, a group of proliferating macrophages (PMs) was identified by their
144 exclusive expression of proliferating markers, *Mki67* and *Birc5* (Fig. S1C).

145 In addition to these well-known types of peritoneal macrophages, three novel
146 subtypes: intermediate “small” macrophages (IMS), intermediate “large”
147 macrophages 1 (IML1), and intermediate “large” macrophages 2 (IML2), were also
148 identified. Cells of IMS showed unique expression of *Folr2* (encodes folate receptor β
149 (FR β) subunit, Fig. 1D). Though cells of IMS showed expression of LPM markers
150 including *Adgre1* (F4/80) and *Icam2* (CD102), equivalent levels of *Retnla* (also
151 known as *Relma* or *Fizz1*), *Mrc1* (CD206), *F13a1*, and *Aif1* as cells of the SPMs were
152 also found in the IMS (Fig. 1D and S1C). These gene expression characteristics of
153 IMS suggest their close developmental relations to SPMs. The other two intermediate
154 groups (IML1 and IML2) showed high expression of *Adgre1* and *Icam2*, but they are
155 low in the expression of *Timd4*, indicating that they are newly recruited immature
156 LPMs.

157 Next, the top 100 differentially expressed genes in each cluster were used to
158 enrich their unique characteristics by gene ontology analysis (GO) of biological
159 processes (Fig. S2 and Table S1). Up-regulated biological processes related to TNF
160 production were found in all three intermediate subtypes (IMS, IML1, and IML2)
161 based on enriched terms of “regulation of tumor necrosis factor production” in IMS,
162 “positive regulation of tumor necrosis factor production” and “negative regulation of
163 transforming growth factor beta production” in IML1, and “tumor necrosis factor
164 production” in IML2. Different from these intermediate subtypes, one term of

165 “regulation of transforming growth factor beta production” was enriched in RLMs,
166 suggesting differential functions between monocyte-derived and embryo-derived
167 macrophages in endometriosis. In addition, the three intermediate groups all show
168 characteristics of “phagocytosis” or “cell killing”, which were not found in the
169 population of RLMs. Different from DC1 and SPMs, enriched biological processes to
170 support the “regulation of angiogenesis” were found in the cells of IMS, IML1, IML2,
171 and RLMs. This high resolution analysis of macrophage transcriptomes identified in
172 our study provides us with an unprecedented opportunity to study stage-specific
173 effects caused by ELL and the treatment of niclosamide.

174

175 **Peritoneal macrophages in a normal physiological state**

176 A publicly-available single-cell RNA-seq dataset from CD11b+ peritoneal
177 macrophages in wild-type female mice in a normal physiological state [GSM4151331,
178 (Bain et al., 2020)] was re-analyzed in this study (Fig. S3A and B). Similar
179 subpopulations related to the “small” peritoneal macrophage lineage were identified
180 and named “DC”, “SPM”, and “IMS”. Four clusters of *Timd4*+ embryo-derived
181 resident macrophages were also identified (RLM1-4). However, different from our
182 samples collected from Sham, ELL, and ELL_N groups, no intermediate “large”
183 (IML) subtypes were distinguished in these macrophages at physiological state.
184 However, their results also support that the continuous differentiation of recruitment
185 macrophages was driven by disrupted homeostasis of macrophages under external
186 stimuli like lesion induction.

187

188 **Niclosamide reverses lesion-induced transcriptomic changes in macrophages**

189 Transcriptomic changes in the macrophages induced by ELL and niclosamide
190 (ELL_N) were compared by the gene set enrichment analysis (GSEA). Compared to
191 the sham group, a total of 135 biological processes were up-regulated by ELL (Fig.
192 2A and Table S2), and 78 of them were reversed by niclosamide (Fig. 2A and Table
193 S2). More specific, ELL induced activation, proliferation, and differentiation of
194 peritoneal macrophages as GO terms of “Establishment or maintenance of cell
195 polarity”, “Transmembrane receptor protein tyrosine kinase signaling pathway”,
196 “Lymphocyte proliferation”, “Positive regulation of cell migration” and “Regulation
197 of lymphocyte differentiation” were all positively enriched compared to the sham
198 group (Fig. 2D). ELL also up-regulated biological processes of “Vesical
199 organization”, “Ceramide transport”, “Regulation of neuron differentiation”, and
200 “Angiogenesis”, which are associated with vascularization, neurogenesis, and pain
201 sensation in lesions. All of the biological processes above were suppressed by
202 niclosamide compared to the ELL group (Fig. 2D). On the other side, 10 out of 12
203 ELL-inhibited pathways were enhanced by niclosamide (Fig. 2B and Table S2). For
204 example, niclosamide promoted biological processes of “Cytoplasmic translation” and
205 “Oxidative phosphorylation” which were reduced by ELL (Fig. 2E and Table S2).

206 Niclosamide tunes disrupted macrophages back to a relevant homeostatic level
207 with the sham group after 3 weeks of treatment (ELL_N/sham), with only 25
208 differential regulated pathways found (Fig. 2C and Table S2). Compared to the sham
209 group, niclosamide further decreased the inflammatory responses and oxidative stress
210 in macrophages but promoted their apoptosis as indicated by enriched GO terms of
211 “Macrophage derived foam cell differentiation”, “I-kappaB kinase/NF-kappaB
212 signaling”, “Cellular response to oxidative stress” and “Negative regulation of
213 apoptotic signaling pathways” (Fig. 2C). These results indicate that ELL induced

214 aberrant activation of macrophages and enhanced their signaling communications for
215 lesion growth and pain sensation, which were finely reversed by niclosamide at the
216 transcriptomic level.

217

218 **Niclosamide suppressed the expression of genes that were enhanced by ELL**

219 To further understand the transcriptomic changes in macrophages caused by ELL and
220 niclosamide, we examined their corresponding alterations at the gene level (Fig. 3A).

221 A total of 116 genes were up-regulated by ELL compared to the sham group
222 (ELL/sham) with 91 of them being decreased by niclosamide (ELL_N/ELL). These
223 top up-regulated genes by the presence of ELL include *Retnla*, *Mrc1*, *F13a1*, *Kctd12*,
224 *Plxnd1*, *Ccl9*, *Ccl6*, and *Socs6*, which were all subsequently inhibited by niclosamide
225 (Fig. 3C). These differentially expressed genes were also confirmed by qPCR
226 analyses in independent samples (Fig. 3D). Consistently, ELL enhanced the
227 expression of *Retnla*, *Mrc1*, *Ccl6*, *Kctd12*, and *Scocs6* while niclosamide suppressed
228 the expression of *Retnla*, *F13a1*, *Mrc1*, *Ccl6* ($p=0.06$), *Kctd12*, *Scocs6*, and *Plxnd1*.
229 Interestingly, most of these up-regulated genes by ELL were uniquely distributed in
230 the populations of DC1, SPMs, and IMS (Fig. 3E) but not the LPMs subtypes (IML1,
231 IML2, RLMs). Consistent with their distributions in our samples, a similar pattern
232 was also found in the re-analyzed dataset of macrophages at the normal physiological
233 state (DC, SPM, and IMS; Fig. S3C). Therefore, ELL enhanced gene expressions
234 related to the lineage of recruited “small” macrophages, and niclosamide reversed
235 those changes.

236

237 **Niclosamide attenuates the recruitment of “small” peritoneal macrophages**

238 As cells from DC1, SPMs, and IMS showed close developmental relations based on
239 their gene expression patterns (Fig. 1D and S1C), the differentiation of cells from
240 DC1 to SPMs and IMS is considered a continuous process. Therefore, we next
241 applied pseudo-temporal trajectory analysis to these three subpopulations to elucidate
242 the dynamic changes and functions of ELL-enhanced genes along this early
243 differentiation process of recruited macrophages. Cells from DC1, SPMs, and IMS
244 were computationally selected, and a continuous trajectory of the differentiation
245 process was constructed using Monocle3 (Fig 4A). The expression of genes enhanced
246 by ELL including *Retnla*, *Mrc1*, *F13a1*, *Kctd12*, *Plxnd1*, *Ccl9*, *Ccl6*, and *Socs6* (Fig.
247 3B and C) were plotted along this developmental timeline (Fig. 4B). Interestingly,
248 most of these genes showed a consistent upregulation pattern during the early
249 differentiation process of SPMs from DC1 (Fig. 4B). This dynamic expression pattern
250 was also confirmed by the re-analyzed datasets of macrophages at physiological states
251 (Fig. S4A and B).

252 Among those genes, the expression of *Retnla* increases by about 100-folds during
253 this process of differentiation (Fig. 4B). The function of *Retnla* for this dynamic
254 process was further studied by *in silico* knockout *Retnla* in these three subpopulations.
255 The top dysregulated genes by virtual knockout of *Retnla* include *Gas6*, *H2-Oa*,
256 *Cd209a*, *Ccr2*, *Il1b*, and *Folr2* (Table S3). Those perturbed genes affected multiple
257 important pathways of immune responses such as biological processes of “leukocyte
258 migration”, “leukocyte chemotaxis”, “phagocytosis”, “regulation of cytokine
259 production involved in immune response”, “antigen processing and presentation” and
260 “regulation of interleukin-2 production” (Fig. 4C and Table S3). In addition, *Retnla*
261 knockout may also affect the communications between macrophages and T cells,
262 shown by GO terms of “T cell activation” and “T cell differentiation”.

263 As ELL enhanced the expression of genes that are necessary for the
264 differentiation of SPMs from DC1, an increased population number of SPMs was
265 expected in the ELL group. By the analysis of flow cytometry, we confirmed a more
266 than 3 times increase in the number of Ly6C+ recruited small macrophages in the
267 group of ELL, which was reduced to a similar level with the sham group by
268 niclosamide (Fig. 4D). As a consequence, the populations of FR β + (encoded by
269 *Folr2*) IMS and CD206+ (encoded by *Mrc1*) recruited macrophages were also
270 increased by ELL and decreased by niclosamide (Fig. 4E). Therefore, niclosamide
271 attenuated the recruitment of macrophages by decreasing its differentiation from DC1,
272 which was promoted by ELL.

273

274 **Niclosamide increased the expression of genes that were decreased by ELL**
275 In addition to niclosamide's suppressions on the genes that were enhanced by ELL,
276 niclosamide also up-regulated over 50% of genes that were reduced by ELL induction
277 (Fig. 3B). The top representative genes include *Cfb*, *Hp*, *Ifitm2*, *Ifitm3*, *Gbp2b*, *C1qb*,
278 *Prdx5*, and *Gngt2* (Fig. 5A). The results of qPCR of immune cells in the peritoneal
279 fluid with different treatments showed consistent changes in the expression of *Cfb*,
280 *Ifitm2*, *Ifitm3*, *Gbp2b*, *C1qb*, *Prdx5*, and *Gngt2* (Fig. 5B). Interestingly, most of these
281 genes were highly expressed in the intermediate subtypes of macrophages and RLMs,
282 but their expression in DC1 and SPMs was very low (Fig. 5C).

283

284 **Niclosamide decreased the maturation of recruited macrophages**
285 Inflammatory conditions lead to the recruitment of LPMs from bone marrow which
286 gradually mature and replenish the resident macrophage pool though they would still
287 be functionally different from those embryo-derived resident macrophages (Louwe et

288 al., 2021). The three subtypes of “large” peritoneal macrophages, IML1, IML2, and
289 RLMs (Fig. 6A) were involved in this biological process of maturation and
290 replenishment and were used to reconstruct a pseudo developmental trajectory (Fig.
291 6A). Then, the down-regulated genes caused by ELL including *Cfb*, *Hp*, *Ifitm2*,
292 *Ifitm3*, *Gbp2b*, *C1qb*, *Prdx5*, and *Gngt2* (Fig. 5A) were plotted along this trajectory
293 path (Fig. 6B). Interestingly, the expression of these genes showed a consistent
294 decreasing pattern during this biological process, suggesting their important roles in
295 maturation inducing.

296 As *Cfb* is one of the most responsive genes regulated by ELL and niclosamide in
297 this biological process (Fig. 5A), we further explored its functions by *in silico*
298 knockout of *Cfb* in cells of IML1, IML2, and RLMs (Table S3). This analysis showed
299 that virtual knockout of *Cfb* not only disrupted the inflammatory responses of
300 macrophages but also changed the metabolism, protein synthesis, and apoptosis of
301 macrophages as terms of “ATP metabolic process”, “Oxidative phosphorylation”,
302 “ribosomal large subunit biogenesis”, and “positive regulation of intrinsic apoptotic
303 signaling pathway” were enriched based on genes disrupted by *Cfb* knockout (Fig. 6C
304 and Table S3). Moreover, *Cfb* seems to be important for TNF production in these
305 LPMs based on enriched terms of “positive regulation on tumor necrosis factor
306 production” (Fig. S2).

307 As no intermediate “large” macrophage phenotypes were identified in the public-
308 available dataset of macrophages at physiological states, no obvious changes of genes
309 mentioned above were found along the trajectory built between those LPMs (LPM1-4,
310 Fig. S5A). This difference also supports the previous finding that the maturation of
311 macrophages is only active upon external stimuli. Therefore, ELL promotes the

312 maturation of recruited macrophages to replenish the resident macrophage pool by
313 downregulating genes such as *Cfb*, and this process is inhibited by niclosamide.

314

315 **Niclosamide reduces the ablation of embryo-derived resident macrophages**

316 The existence of embryo-derived RLMs prohibits the replenishment of the resident
317 macrophage pool by recruited ones, while increased inflammation leads to ablation of
318 embryo-derived RLMs and promotes the process of replenishment (Louwe et al.,
319 2021). In support of this, ELL decreased the expression of *Timd4* and *Apoc1*, markers
320 for embryo-derived RLMs, in the peritoneal macrophages (Fig. 7A and B).

321 Expression of *Timd4* and *Apoc1* was also found to increase along with the initial
322 maturation process of intermediate macrophages, suggesting recruited macrophages
323 also gradually acquire their residency (Fig. 7C). Furthermore, knockout of *Timd4* in
324 these LPM populations was shown to induce their B cell characteristics as terms of “B
325 cell activation”, “B cell receptor signaling pathway” and “B cell proliferation” were
326 enriched based on disrupted genes of *Timd4* knockout (Fig. 7D and Table S3).

327 Knockout *Timd4* also induced changes in TNF production, phagocytosis, and
328 oxidative stress in those “large” types of macrophages.

329 As a consequence of reduced *Timd4* expression in macrophages by ELL, the
330 population number of TIM4+ RLMs was also reduced (Fig. 7E). Niclosamide rescued
331 the expression of *Timd4* and also the number of TIM4+ RLMs (Fig. 7E). Thus, ELL
332 enhanced the replenishment of the resident macrophage pool by increasing the
333 ablation of embryo-derived RLMs, which further promotes the maturation of recruited
334 macrophages. Niclosamide preserves these embryo-derived RLMs by enhancing
335 *Timd4* expression and recuses the homeostasis of macrophages disrupted by ELL.

336

337 **Niclosamide rescues the communications between macrophages and B cells**

338 CXCL13-producing embryo-derived RLMs play an important role in the maintenance
339 and recruitment of peritoneal B1 cells upon inflammation, while newly recruited
340 macrophages were reported to be deficient in CXCL13 (Bain et al., 2020; Beattie et
341 al., 2016; Louwe et al., 2021; Zeng et al., 2018). To understand the communications
342 between macrophages and B cells among their subpopulations, two important
343 signaling networks for immune cell recruitment, CXCL and CCL, were analyzed
344 based on the ligand and receptor interactions between cells using the CellChat
345 package. Most of the CCL ligands were found to be released by macrophages and
346 received by themselves, whereas there were very few communications between
347 macrophages and B cells (Fig. 8A). The SPMs were the most affected cells by the
348 CCL signaling from the other types of macrophages, which is consistent with their
349 increased recruitment by ELL induction.

350 On the other hand, the expression of CXCL ligands was found to be mostly
351 expressed in “large” types of macrophages, such as IML1, IML2, and RLMs, and
352 signals received by B cells (Fig. 8B). Furthermore, we explored the interactions
353 between these CXCL-producing “large” types of macrophages and the three largest
354 populations of B cells (B1a, B1b, and B2). Twenty-three significantly expressed
355 ligand-receptor pairs were identified including *App-Cd74*, *Cxcl13-Cxcr5*, *C3-Cr2*,
356 *Fn1-Sdc4*, *Ptprc-Cd22*, which may play important roles in the recruitment and
357 functionality of B cells under the inflammatory condition induced by ELL induction.
358 Among them, decreased expression of *Cxcl13* and *C3* was found in the peritoneal
359 macrophages by ELL, and their expression was enhanced by niclosamide (Fig. 8D).
360 Moreover, B1a and B1b cells received the most *Cxcl13* signals, while B2 cells
361 exclusively received the signals of *C3* (Fig. 8C). In addition, the expression of *Fn1*

362 and *Ptprc* in macrophages was also altered by ELL and niclosamide ($p<0.05$), but the
363 changes are limited.

364 The transcriptomic changes caused by ELL and niclosamide to B cells were also
365 analyzed. Compared to the macrophages, the overlaps of biological processes that
366 were disrupted by ELL (ELL/sham) and reversed by niclosamide (ELL_N/ELL) were
367 much fewer (Figs. 8E and F; Table S4). Only 28 out of 114 biological processes that
368 were enhanced by ELL were reversed by niclosamide (Fig. 8F; Table S4). The limited
369 overlaps include biological processes of “response to growth factor” and “homeostasis
370 of number of cells” (Fig. 8G), which may be associated with the recruitment and
371 maintenance of the number of B cells through macrophages.

372 These results suggest that ELL disrupted the communications between “large”
373 types of macrophages and B1/B2 cells, which were rescued by niclosamide through
374 up-regulating the expression of *Cxcl13* and *C3*. The transcriptomic alternations
375 caused by niclosamide to B cells are minimal, indicating that macrophages are
376 possibly the direct targets of niclosamide.

377

378 **Discussion**

379 Niclosamide is an FDA-approved oral anthelmintic drug that is originally used to treat
380 human tapeworm infections (Selection et al., 2014). In addition to this common use,
381 many clinical studies are ongoing to repurpose niclosamide for the treatment of other
382 diseases such as different types of cancer, bacterial and viral infections, neuropathic
383 pain, systemic sclerosis, and metabolic diseases (Chen et al., 2018; Fonseca et al.,
384 2012; Jurgeit et al., 2012; Morin et al., 2016; Osada et al., 2011; Tao et al., 2014; You
385 et al., 2014; Zhang et al., 2013). Though the clear direct binding targets of
386 niclosamide have not been identified, studies have shown that niclosamide affects

387 multiple important signaling pathways. One of the most appreciated action
388 mechanisms is that niclosamide acts as a protonophore and thus uncouples oxidative
389 phosphorylation and affects pH balance in cells (Chen et al., 2018; Jurgeit et al., 2012;
390 Tao et al., 2014). In addition, signaling pathways of mTOR, Wnt/β-catenin, STAT3,
391 NF-κB, and Notch are also modulated by niclosamide (Fonseca et al., 2012; Jin et al.,
392 2010; King et al., 2015; Wang et al., 2009; You et al., 2014; Zhang et al., 2013). In
393 endometriosis, we also found that niclosamide reduced the growth of lesions and
394 decreased inflammation at lesions through its suppression of STAT3 and NF-κB
395 signaling (Prather et al., 2016; Sekulovski et al., 2019; Sekulovski et al., 2020).
396 Moreover, we also found that niclosamide does not disrupt reproductive functions in
397 mice, making it a relatively safe drug for treatment (Prather et al., 2016).

398 Abnormal activation and increased numbers of macrophages along with elevated
399 levels of proinflammatory cytokines such as IL-1 β , IL6, IL8, and TNF α were found in
400 the peritoneal fluid of patients with endometriosis (Milewski et al., 2008; Scholl et al.,
401 2009; Zhou et al., 2020). We also reported that niclosamide treatment reduced
402 inflammation in the peritoneal fluid as well as lesions, pelvic organs (uterus and
403 vagina), and dorsal root ganglion (Shi et al., 2021). Consequently, niclosamide also
404 decreased macrophage infiltration, vascularization, and innervation in the
405 endometriotic lesions (Shi et al., 2021). In this study, we further reported that most of
406 the transcriptomic changes in peritoneal macrophages induced by ELL were rescued
407 by niclosamide. These changes include necessary biological processes for
408 macrophage activation and for its communications with other types of cells, such as
409 processes to promote angiogenesis and neurogenesis. Consistent with the unique
410 function of niclosamide for mitochondria uncoupling, the biological processes of
411 oxidative phosphorylation in macrophages were promoted by niclosamide.

412 Furthermore, niclosamide rescues disrupted macrophage subpopulations back to a
413 similar transcriptomic level compared with those in the sham group and further
414 reduced the signaling of NF- κ B and oxidative stress, and promoted apoptosis in
415 macrophages after 3 weeks of treatment.

416 Previous studies have suggested the long-term existence of transitory
417 macrophages in the peritoneal cavity under inflammation in addition to traditionally
418 recognized SPMs and LPMs, but our knowledge of those immature subtypes and their
419 contributions to disease development is limited (Bain et al., 2020; Liu et al., 2019;
420 Louwe et al., 2021). In this study, we further characterized these subpopulations and
421 identified three intermediate immature subtypes, named IMS, IML1, and IML2. Cells
422 of the IMS showed close developmental relationships with SPMs with high
423 expression of *Retnla* (*Relma* or *Fizz1*), *Mrc1* (CD206), *F13a1*, and *Aif1*, which are
424 important markers for monocyte-derived cells (Elizondo et al., 2019; Lee et al., 2014;
425 Porrello et al., 2018; Yu et al., 2020). The populations of IML1 and IML2 are quite
426 similar in transcriptomes and are F4/80^{high} MHC II^{low}, but both of them are low in the
427 expression of *Timd4*, suggesting that they are newly recruited LPMs. All three
428 intermediate groups were characterized by TNF production, while the embryo-derived
429 RLMs are supportive of TGF β production. In addition to TNF production, cells of
430 IMS also support angiogenesis. Therefore, their prolonged existence by ELL may
431 promote lesion growth.

432 Under a successful resolution of inflammation, the recruited SPMs decrease their
433 numbers by apoptosis or migrating to local draining lymph nodes (Bellingan et al.,
434 1996; Gautier et al., 2013). However, under persistent inflammation, some of the
435 recruited SPMs eventually differentiate into F4/80^{high} MHC II^{low} cells, which
436 corresponds to the intermediate subtypes identified in this study (Bain et al., 2016;

437 Yona et al., 2013). Consistently, by constructing a continuous developmental
438 trajectory using cells of DC1, SPMs, and IMS, we reported that ELL-induced
439 inflammation promoted the differentiation of SPMs from DC1 by increasing the
440 expression of genes necessary for this process. Moreover, our analysis strongly
441 suggests that *Retnla* is a potential key driver for this process. In support of this,
442 reduced expression of *Retnla* by niclosamide suppressed this early differentiation
443 process and led to reduced populations of both recruited Ly6C⁺ monocytes and more
444 differentiated FR β ⁺ IMS, indicating that niclosamide is able to improve persistent or
445 chronic information that is developed by lesion establishment.

446 Severe inflammation results in the ablation of embryo-derived RLMs and
447 increases the replenishment of RLMs by monocyte-derived macrophages (Louwe et
448 al., 2021). The two populations of IML1 and IML2 are in the transition to acquiring
449 their long-term residence as embryo-derived RLMs. By constructing a maturation
450 process of IML1 and IML2, we found that ELL decreased the expression of necessary
451 genes such as *Cfb* to promote, while niclosamide enhanced most of these gene
452 expressions to reverse this replenishment process. Moreover, both the expression of
453 *Timd4* and the cell number of TIM4⁺ RLMs were decreased by ELL and increased by
454 niclosamide. Therefore, niclosamide prohibited the replenishment of resident
455 macrophages by both suppressing the maturation of monocyte-derived macrophages
456 and preserving the population of embryo-derived RLMs. As the monocyte-derived
457 RLMs were reported to have different functions from original RLMs, enhanced
458 replenishment of resident macrophages may have long-term disruptions to the
459 peritoneal niche of endometriosis (Louwe et al., 2021).

460 CXCL13 expression in TIM4⁺ RLMs plays an essential role in the maintenance
461 and recruitment of B1 cells from circulation (Beattie et al., 2016; Zeng et al., 2018).

462 However, the expression of CXCL13 is deficient in monocyte-derived RLMs, which
463 leads to disruption of B1 cell homeostasis under inflammation (Bain et al., 2020;
464 Louwe et al., 2021). We found that CXCL13 was actually expressed in all LPMs
465 (IML1, IML2, and RLMs). But, consistently, we found that ELL decreased the cell
466 number of TIM4+ RLMs, and the expression of CXCL13 in macrophages.
467 Niclosamide promoted the expression of CXCL13 and rescued the communications of
468 macrophages to B1 cells. In addition, intercellular interaction analysis also suggested
469 that the three “large” types of macrophage populations might also regulate the
470 population of B2 cells by the *C3* expression. Treatment of niclosamide enhanced the
471 expression of *C3*. Therefore, ELL might disrupt the communications between LPMs
472 and B1 and B2 cells, and niclosamide could rescue this communication through its
473 regulations on macrophages.

474 In summary, the heterogeneity and developmental characteristics of peritoneal
475 macrophages were extensively explored this study using a mouse model of
476 endometriosis. ELL enhanced the process of early differentiation and maturation of
477 monocyte-derived macrophages while reducing the maintenance of embryo-derived
478 RLMs. The increased replenishment of resident macrophages by monocyte-derived
479 ones further disrupts the homeostasis in the peritoneal cavity and affects the
480 recruitment and functional activities of B cells. Niclosamide stepwise reverses the
481 dynamic progression of recruited macrophages and preserves the population of
482 embryo-derived RLMs, hence tuning the perturbed peritoneal microenvironment in
483 endometriosis back to normal. Therefore, macrophages could be a direct target of
484 niclosamide, and niclosamide could be a new therapy to recuse perturbed peritoneal
485 microenvironment that contributes to chronic inflammation, lesion growth, and
486 progression, neuroangiogenesis, and endometriosis-associate pain.

487

488 **Materials and methods**

489

490 **Animals and a mouse model of endometriosis**

491 All procedures were performed in accordance with the guidelines approved by the
492 Institutional Animal Care and Use Committee of the Washington State University
493 (Protocol # 6751). C57BL/6J mice were purchased from the Jackson Laboratory.
494 Endometriosis-like lesions (ELL) were induced by inoculating syngeneic menstrual-
495 like endometrial fragments from donor mice into the peritoneal cavity of recipient
496 mice, as described previously (Greaves et al., 2014; Shi et al., 2021). Briefly,
497 ovariectomized donor mice were primed with estradiol-17 β (E2) and progesterone and
498 induced decidualization by injecting sesame oil into uterine horns to produce a
499 “menses-like” event. Then, decidualized endometrial tissues were scraped from
500 myometrium, minced, and injected i.p. into ovariectomized and E2-primed recipient
501 mice under anesthesia (50 mg tissue in 0.2 mL PBS per recipient). Sham mice were
502 ovariectomized and E2-primed and injected with 0.2 mL PBS into the peritoneal
503 cavity. Three weeks after the induction of ELL or sham, mice in the groups of sham,
504 ELL, and ELL_N were orally administrated with vehicle or niclosamide (200
505 mg/kg/day) for a total of 3 weeks (Fig. 1A), as described previously (Shi et al., 2021).
506 At 6 weeks following ELL induction, mice were euthanized, and peritoneal cells were
507 collected for further analysis.

508

509 **Preparation of peritoneal immune cells for single-cell RNA sequencing**

510 Peritoneal immune cells were isolated and collected from the peritoneal fluid
511 following our established method (Shi et al., 2021). After removing red blood cells by

512 lysis, remaining cell mixtures were used for cDNA library constructions following the
513 manufacturer's protocol (10X Genomics, Inc.) of the Chromium Single Cell 3'
514 Library & Gel Bead Kit V3 (Zhao et al., 2021). All samples were multiplexed
515 together and sequenced across one single lane of an Illumina NovaSeq 6000 S4.

516

517 **Single-cell data processing and analysis**

518 Raw data in FASTQ format were pre-processed with Cell Ranger V3.1.0 (10x
519 Genomics) mapping to the mouse GRCm38/mm10 transcriptome to generate gene-
520 cell matrices. A total of 13,859 cells from all three libraries were integrated into R
521 using the Seurat package (V4.0.4) (Stuart et al., 2019). To filter out doublets and low-
522 quality cells, criteria of 750,000 unique molecular identifiers (UMIs) and 500 genes
523 per cell were set. In addition, cells with over 20% expression of mitochondrial genes
524 were excluded for downstream analysis. Modified multivariate Pearson's RV
525 correlations for each set of treatment replicates were calculated using the package of
526 MatrixCorrelation (v0.9.2) (Smilde et al., 2009). The following correlations showed
527 consistent sampling between libraries of treatments: ELL and sham = 0.962, ELL_N
528 and sham = 0.979, ELL and ELL_N = 0.985. The “sctransform” function was then
529 applied to normalize the remaining dataset with regression of mitochondria mapping
530 percentage (Hafemeister and Satija, 2019). Dimensionality reduction was performed
531 on identified variable genes by principal component analyses (PCA). The top 66
532 dimensions were selected for clustering (“resolution” set to 0.5) and uniform manifold
533 approximation and projection (UMAP) visualization. Specific gene markers for each
534 cluster were identified using the “FindAllMarkers” function. Differential gene
535 expression between treatments was analyzed using the “wilcox” test in the
536 “FindMarkers” function with Bonferroni adjusted p value < 0.05 showing significant

537 differences. Gene Ontology (GO) and Gene Set Enrichment Analysis (GSEA) was
538 performed with the R package, clusterProfiler V3.18.0, using all detected genes from
539 the entire scRNA-seq library as background (Yu et al., 2012). Terms were enriched
540 with the nominal *p* value < 0.05 and false discovery rate (FDR) (*q* value) < 0.05.

541

542 **An interactive web tool to share scRNA-seq data of peritoneal immune cells**

543 Single-cell transcriptomic analysis has provided an unprecedented high resolution of
544 peritoneal immune cells including different subtypes of B cells, macrophages, and T
545 cells. To share our data with other researchers, we have created a cloud-based web
546 tool for easy gene searches, which does not require complicated computer
547 programming skills (Thompson et al., 2021). The webpage for this tool is:

548 <https://kanakohayashilab.org/hayashi/en/mouse/peritoneal.immune.cells/>

549

550 **Single-cell trajectory analysis**

551 The biological processes of “small” macrophage recruitment and “large” macrophage
552 maturation were revealed by the trajectory analysis. Cells from clusters of DC1,
553 SPMs, and IMS or IML1, IML2, and RLMs were computationally selected in Seurat,
554 and the two data matrices were imported, processed, and pseudo-ordered using the
555 package of Monocle 3 in R following the standard pipeline (Qiu et al., 2017).

556

557 ***In Silico* Knockout Analysis**

558 Functional analysis of *Retnla*, *Cfb*, and *Timd4* was conducted using the R package of
559 scTenifoldKnn V1.0.1 (Osorio et al., 2022). A single-cell gene regulatory network
560 (scGRN) was conducted using our scRNA-seq data from the sham group. Then the
561 expression of *Retnla*, *Cfb*, and *Timd4* was set to zero from the constructed scGRN to

562 build their own corresponding “pseudo-knockout” scGRN. Perturbed genes by this
563 virtual knockout were quantified by comparison of the “pseudo-knockout” scGRN to
564 the original scGRN. Those significantly affected genes were used for GO analysis to
565 show changes in biological processes caused by *in silico* knockout.

566

567 **Intercellular Communication Analysis**

568 Gene expression data of Seurat objects were used as input to model the probability of
569 intercellular interactions between B cells and macrophages using the R package of
570 CellChat V1.0.0 (Jin et al., 2021). The known database of interactions
571 (CellChat.DB.mouse) between ligands, receptors, and cofactors was used as the
572 reference.

573

574 **Re-analysis of one public-available single-cell dataset of peritoneal macrophages**

575 A single-cell transcriptomic dataset of peritoneal macrophages from 19-weeks old
576 female mice is public available (Bain et al., 2020). These cells were selected based on
577 the expression of CD11b with the removal of granulocytes and B1 B cells using flow
578 cytometry. The raw data were downloaded from NCBI GEO (GSM4151331), pre-
579 processed with Cell Ranger V3.1.0, and re-analyzed in the R package, Seurat V4.0.4.
580 For quality control, cells with the expression of fewer than 300 genes or over 5000
581 genes, and over 5% mitochondrial genes were excluded, resulting in a total of 4287
582 out of 4702 cells for downstream analysis. Following the standard pipeline of Seurat,
583 the raw counts were normalized using a global-scaling normalization method
584 (“LogNormalize”). Using the “ScaleData” function, the normalized dataset was
585 further scaled for dimensional reduction. Based on the principal component analyses
586 (PCA), the top 34 dimensions were selected for clustering and UMAP graphing.

587 Trajectory analysis was performed on the cells computationally selected from the
588 “small” or “large” macrophage lineages as described above using the R package of
589 Monocle 3.

590

591 **Flow Cytometry**

592 Peritoneal cells were harvested and used for analyzing immune cell profiles by flow
593 cytometry. Briefly, the peritoneal lavages were centrifuged to collect peritoneal
594 exudate cells. After lysing red blood cells by 1x RBC Lysis Buffer (BioLegend), an
595 equal number of cells from each group were incubated at room temperature for 20
596 minutes with Zombie Aqua™ Fixable Viability dye (BioLegend) and blocked on ice
597 for 20 minutes with FcBlock anti-CD16/CD32 (Thermo Fisher). Then cells were
598 stained with fluorochrome-conjugated monoclonal antibodies (Table S1) for 1 hour.
599 Samples were acquired with the Attune NxT Acoustic Focusing Cytometer using
600 Attune NxT software (Invitrogen), and data were analyzed with FlowJo v10.4. For
601 analysis, only singlets (determined by forward scatter height vs. area) and live cells
602 (Zombie Aqua negative) were used.

603

604 **Quantitative Real-time PCR Analyses (qPCR)**

605 Total RNA was isolated using TRIzol reagent (Sigma #T9424), and cDNA templates
606 were synthesized from 1 μ g of purified RNA using the High-Capacity cDNA Reverse
607 Transcription Kit (Thermo Fisher) (Shi et al., 2021; Zhao et al., 2020). qPCR was
608 performed using a CFX RT-PCR detection system (Bio-Rad), and relative gene
609 expression was evaluated by SYBR Green (Bio-Rad #1725274) incorporation. *Rpl19*
610 was used as the reference gene to normalize mRNA expression levels. Data were
611 analyzed using the $2^{-\Delta\Delta C_t}$ method. Primer sequences were provided in Table S2.

612

613 **Statistical Analysis**

614 For single-cell transcriptomic sequencing, in each treatment, a total of 3 mice were
615 used for sample preparation. Pre-processing of raw sequencing data including
616 transformation, normalization, and quality control were described above. For the
617 analysis of differential gene expression, the default “wilcox” test was performed using
618 the R package Seurat (v4.0.4). For RT-qPCR of peritoneal immune cells, six mice
619 from each treatment were used for RNA extraction (n=6). For flow cytometry, cells
620 from three mice were pooled as one sample and a total of 15 mice were used for each
621 group of treatments (n=5). For comparisons between three groups of treatments, one-
622 way ANOVA followed by Tukey's multiple comparisons was used. Data were
623 analyzed with GraphPad Prism (version 9) and presented as means \pm SEM. Statistical
624 differences were indicated as $*p < 0.05$, $**p < 0.01$, $***p < 0.001$.

625

626 **Data availability**

627 The data that support the findings of this study are openly available in the GEO
628 database at NCBI, reference number GSE147024.

629

630 **Acknowledgments**

631 The study was supported by the National Institutes of Health (NIH), Eunice Kennedy
632 Shriver National Institute of Child Health & Human Development (NICHD)
633 R01HD104619 (to K. Hayashi). The graphical abstract was created using
634 BioRender.com.

635

636 Author contributions: M. Shi and K. Hayashi designed experiments. L. Zhao and M.
637 Shi performed experiments and analyzed data. S. Winuthayanon assisted with the
638 webtool constructions and technical support with data analysis. J. A. MacLean and K.
639 Hayashi assisted in experiments and provided critical feedback on the manuscript. L.
640 Zhao wrote the paper. All authors read, edited, and approved the manuscript.

641

642 **Online supplementary material**

643 **Figure S1** shows the characteristic gene expression of immune cells at the single-cell
644 level. **Figure S2** shows characteristic profiles of each macrophage subpopulation.
645 **Figure S3** shows the re-analysis of a single-cell transcriptomic dataset of peritoneal
646 macrophages in female mice in a normal physiological state from a public resource.
647 **Figure S4** shows the construction of a trajectory path for the differentiation of
648 recruited macrophages (data from a public resource). **Figure S5** shows the
649 construction of a trajectory path for “large” macrophages. **Table S1** shows enriched
650 GO terms of biological processes in each macrophage subpopulation. **Table S2** shows
651 enriched GSEA terms of biological processes in macrophages between treatments.
652 **Table S3** shows genes and GO biological processes affected by *in silico* knockout of
653 *Retnla*, *Cfb*, and *Timd4*. **Table S4** shows enriched GSEA terms of biological
654 processes in B cells between treatments. **Table S5** shows antibodies and reagents for
655 Flow Cytometry. **Table S6** shows primer information used for RT-qPCR.

656 References

657 Bacci, M., A. Capobianco, A. Monno, L. Cottone, F. Di Puppo, B. Camisa, M. Mariani, C. Brignole, M.
658 Ponzoni, and S. Ferrari. 2009. Macrophages are alternatively activated in patients with
659 endometriosis and are required for the growth and vascularization of lesions in a mouse model
660 of disease. *The American journal of pathology* 175:547-556.

661 Bain, C., D. Gibson, N. Steers, K. Boufea, P. Louwe, C. Doherty, V. González-Huici, R. Gentek, M.
662 Magalhaes-Pinto, and T. Shaw. 2020. Rate of replenishment and microenvironment contribute
663 to the sexually dimorphic phenotype and function of peritoneal macrophages. *Science
664 immunology* 5:eabc4466.

665 Bain, C.C., C.A. Hawley, H. Garner, C.L. Scott, A. Schridde, N.J. Steers, M. Mack, A. Joshi, M. Guilliams,
666 and A.M.I. Mowat. 2016. Long-lived self-renewing bone marrow-derived macrophages
667 displace embryo-derived cells to inhabit adult serous cavities. *Nature communications* 7:1-14.

668 Beattie, L., A. Sawtell, J. Mann, T.C. Frame, B. Teal, F. de Labastida Rivera, N. Brown, K. Walwyn-Brown,
669 J.W. Moore, and S. MacDonald. 2016. Bone marrow-derived and resident liver macrophages
670 display unique transcriptomic signatures but similar biological functions. *J Hepatol* 65:758-768.

671 Bellingan, G.J., H. Caldwell, S. Howie, I. Dransfield, and C. Haslett. 1996. In vivo fate of the inflammatory
672 macrophage during the resolution of inflammation: inflammatory macrophages do not die
673 locally, but emigrate to the draining lymph nodes. *The Journal of Immunology* 157:2577-2585.

674 Capobianco, A., and P. Rovere Querini. 2013. Endometriosis, a disease of the macrophage. *Front.
675 Immunol.* 4:9.

676 Chen, W., R.A. Mook Jr, R.T. Premont, and J. Wang. 2018. Niclosamide: Beyond an antihelminthic drug.
677 *Cell. Signalling* 41:89-96.

678 Cheong, Y., J. Shelton, S. Laird, M. Richmond, G. Kudesia, T. Li, and W. Ledger. 2002. IL-1, IL-6 and TNF-
679 α concentrations in the peritoneal fluid of women with pelvic adhesions. *Hum Reprod* 17:69-
680 75.

681 De Ziegler, D., B. Borghese, and C. Chapron. 2010. Endometriosis and infertility: pathophysiology and
682 management. *The Lancet* 376:730-738.

683 Ding, S., X. Guo, L. Zhu, J. Wang, T. Li, Q. Yu, and X. Zhang. 2021. Macrophage-derived netrin-1
684 contributes to endometriosis-associated pain. *Annals of Translational Medicine* 9:

685 Elizondo, D.M., N.Z.D. Brandy, R.L.L. da Silva, N.L. Haddock, A.D. Kacsinta, T.R. de Moura, and M.W.
686 Lipscomb. 2019. Allograft Inflammatory Factor-1 Governs Hematopoietic Stem Cell
687 Differentiation Into cDC1 and Monocyte-Derived Dendritic Cells Through IRF8 and RelB in vitro.
688 *Front. Immunol.* 10:

689 Fonseca, B.D., G.H. Diering, M.A. Bidinosti, K. Dalal, T. Alain, A.D. Balgi, R. Forestieri, M. Nodwell, C.V.
690 Rajadurai, and C. Gunaratnam. 2012. Structure-activity analysis of niclosamide reveals
691 potential role for cytoplasmic pH in control of mammalian target of rapamycin complex 1
692 (mTORC1) signaling. *Journal of Biological Chemistry* 287:17530-17545.

693 Forster, R., A. Sarginson, A. Velichkova, C. Hogg, A. Dornig, A.W. Horne, P.T. Saunders, and E. Greaves.
694 2019. Macrophage - derived insulin - like growth factor - 1 is a key neurotrophic and nerve -
695 sensitizing factor in pain associated with endometriosis. *The FASEB Journal* 33:11210-11222.

696 Gautier, E.L., S. Ivanov, P. Lesnik, and G.J. Randolph. 2013. Local apoptosis mediates clearance of
697 macrophages from resolving inflammation in mice. *Blood, The Journal of the American Society
698 of Hematology* 122:2714-2722.

699 Ghosn, E.E.B., A.A. Cassado, G.R. Govoni, T. Fukuhara, Y. Yang, D.M. Monack, K.R. Bortoluci, S.R.
700 Almeida, L.A. Herzenberg, and L.A. Herzenberg. 2010. Two physically, functionally, and
701 developmentally distinct peritoneal macrophage subsets. *Proceedings of the National
702 Academy of Sciences* 107:2568-2573.

703 Greaves, E., F.L. Cousins, A. Murray, A. Esnal-Zufiurre, A. Fassbender, A.W. Horne, and P.T. Saunders.
704 2014. A novel mouse model of endometriosis mimics human phenotype and reveals insights
705 into the inflammatory contribution of shed endometrium. *The American journal of pathology*
706 184:1930-1939.

707 Greaves, E., J. Temp, A. Esnal-Zufiurre, S. Mechsner, A.W. Horne, and P.T. Saunders. 2015. Estradiol is
708 a critical mediator of macrophage-nerve cross talk in peritoneal endometriosis. *The American
709 journal of pathology* 185:2286-2297.

710 Hafemeister, C., and R. Satija. 2019. Normalization and variance stabilization of single-cell RNA-seq data
711 using regularized negative binomial regression. *Genome Biol.* 20:1-15.

712 Hogg, C., A.W. Horne, and E. Greaves. 2020. Endometriosis-Associated Macrophages: Origin, Phenotype,
713 and Function. *Frontiers in Endocrinology* 11:

714 Hogg, C., K. Panir, P. Dhami, M. Rosser, M. Mack, D. Soong, J.W. Pollard, S.J. Jenkins, A.W. Horne, and
715 E. Greaves. 2021. Macrophages inhibit and enhance endometriosis depending on their origin.
716 *Proceedings of the National Academy of Sciences* 118:

717 Jin, S., C.F. Guerrero-Juarez, L. Zhang, I. Chang, R. Ramos, C.-H. Kuan, P. Myung, M.V. Plikus, and Q. Nie.
718 2021. Inference and analysis of cell-cell communication using CellChat. *Nature
719 Communications* 12:1088.

720 Jin, Y., Z. Lu, K. Ding, J. Li, X. Du, C. Chen, X. Sun, Y. Wu, J. Zhou, and J. Pan. 2010. Antineoplastic
721 mechanisms of niclosamide in acute myelogenous leukemia stem cells: inactivation of the NF-
722 kB pathway and generation of reactive oxygen species. *Cancer Res* 70:2516-2527.

723 Johan, M.Z., W.V. Ingman, S.A. Robertson, and M.L. Hull. 2019. Macrophages infiltrating endometriosis-
724 like lesions exhibit progressive phenotype changes in a heterologous mouse model. *J Reprod
725 Immunol* 132:1-8.

726 Jurgeit, A., R. McDowell, S. Moese, E. Meldrum, R. Schwendener, and U.F. Greber. 2012. Niclosamide is
727 a proton carrier and targets acidic endosomes with broad antiviral effects. *PLoS Path.*
728 8:e1002976.

729 Kim, K.-W., J.W. Williams, Y.-T. Wang, S. Ivanov, S. Gilfillan, M. Colonna, H.W. Virgin, E.L. Gautier, and
730 G.J. Randolph. 2016. MHC II+ resident peritoneal and pleural macrophages rely on IRF4 for
731 development from circulating monocytes. *J Exp Med* 213:1951-1959.

732 King, M.L., M.E. Lindberg, G.R. Stodden, H. Okuda, S.D. Ebers, A. Johnson, A. Montag, E. Lengyel, J.
733 MacLean li, and K. Hayashi. 2015. WNT7A/β-catenin signaling induces FGF1 and influences
734 sensitivity to niclosamide in ovarian cancer. *Oncogene* 34:3452-3462.

735 Lee, M.-R., C.-j. Lim, Y.-H. Lee, J.-G. Park, S.K. Sonn, M.-N. Lee, I.-H. Jung, S.-J. Jeong, S. Jeon, and M. Lee.
736 2014. The adipokine Retnla modulates cholesterol homeostasis in hyperlipidemic mice. *Nature
737 communications* 5:1-15.

738 Liu, Z., S. Chen, C. Qiu, Y. Sun, W. Li, J. Jiang, and J.-M. Zhang. 2018. Fractalkine/CX3CR1 contributes to
739 endometriosis-induced neuropathic pain and mechanical hypersensitivity in rats. *Front. Cell.
740 Neurosci.* 12:495.

741 Liu, Z., Y. Gu, S. Chakarov, C. Bleriot, I. Kwok, X. Chen, A. Shin, W. Huang, R.J. Dress, and C.-A. Dutertre.
742 2019. Fate mapping via Ms4a3-expression history traces monocyte-derived cells. *Cell*
743 178:1509-1525. e1519.

744 Louwe, P., L. Badiola Gomez, H. Webster, G. Perona-Wright, C. Bain, S. Forbes, and S. Jenkins. 2021.
745 Recruited macrophages that colonize the post-inflammatory peritoneal niche convert into
746 functionally divergent resident cells. *Nature communications* 12:1-15.

747 Milewski, Ł., E. Barcz, P. Dziunycz, D. Radomski, P. Kamiński, P.I. Roszkowski, G. Korczak-Kowalska, and
748 J. Malejczyk. 2008. Association of leptin with inflammatory cytokines and lymphocyte
749 subpopulations in peritoneal fluid of patients with endometriosis. *J Reprod Immunol* 79:111-
750 117.

751 Morin, F., N. Kavian, C. Nicco, O. Cerles, C. Chéreau, and F. Batteux. 2016. Niclosamide prevents
752 systemic sclerosis in a reactive oxygen species-induced mouse model. *The Journal of
753 Immunology* 197:3018-3028.

754 Osada, T., M. Chen, X.Y. Yang, I. Spasojevic, J.B. Vandeusen, D. Hsu, B.M. Clary, T.M. Clay, W. Chen, and
755 M.A. Morse. 2011. Antihelminth compound niclosamide downregulates Wnt signaling and
756 elicits antitumor responses in tumors with activating APC mutations. *Cancer Res* 71:4172-4182.

757 Osorio, D., Y. Zhong, G. Li, Q. Xu, Y. Yang, Y. Tian, R.S. Chapkin, J.Z. Huang, and J.J. Cai. 2022.
758 scTenifoldKnk: An efficient virtual knockout tool for gene function predictions via single-cell
759 gene regulatory network perturbation. *Patterns* 100434.

760 Porrello, A., P.L. Leslie, E.B. Harrison, B.K. Gorentla, S. Kattula, S.K. Ghosh, S.H. Azam, A. Holtzhausen,
761 Y.L. Chao, M.C. Hayward, T.A. Waugh, S. Bae, V. Godfrey, S.H. Randell, C. Oderup, L. Makowski,
762 J. Weiss, M.D. Wilkerson, D.N. Hayes, H.S. Earp, A.S. Baldwin, A.S. Wolberg, and C.V. Pecot.
763 2018. Factor XIIIa-expressing inflammatory monocytes promote lung squamous cancer
764 through fibrin cross-linking. *Nature Communications* 9:1988.

765 Prather, G.R., J.A. MacLean, M. Shi, D.K. Boadu, M. Paquet, and K. Hayashi. 2016. Niclosamide as a
766 potential nonsteroidal therapy for endometriosis that preserves reproductive function in an
767 experimental mouse model. *Biol Reprod* 95:74, 71-11.

768 Qiu, X., Q. Mao, Y. Tang, L. Wang, R. Chawla, H.A. Pliner, and C. Trapnell. 2017. Reversed graph
769 embedding resolves complex single-cell trajectories. *Nat. Methods* 14:979-982.

770 Rasheed, H.A.M., and P. Hamid. 2020. Inflammation to Infertility: Panoramic View on Endometriosis.
771 *Cureus* 12:

772 Rosas, M., L.C. Davies, P.J. Giles, C.-T. Liao, B. Kharfan, T.C. Stone, V.B. O'Donnell, D.J. Fraser, S.A. Jones,
773 and P.R. Taylor. 2014. The transcription factor Gata6 links tissue macrophage phenotype and
774 proliferative renewal. *Science* 344:645-648.

775 Scholl, B., N.A. Bersinger, A. Kuhn, and M.D. Mueller. 2009. Correlation between symptoms of pain and
776 peritoneal fluid inflammatory cytokine concentrations in endometriosis. *Gynecol Endocrinol*
777 25:701-706.

778 Sekiguchi, K., Y. Ito, K. Hattori, T. Inoue, K. Hosono, M. Honda, A. Numao, H. Amano, M. Shibuya, and N.
779 Unno. 2019. VEGF receptor 1-expressing macrophages recruited from bone marrow enhances
780 angiogenesis in endometrial tissues. *Scientific reports* 9:1-14.

781 Sekulovski, N., A.E. Whorton, M. Shi, J.A. MacLean, and K. Hayashi. 2019. Endometriotic inflammatory
782 microenvironment induced by macrophages can be targeted by niclosamide. *Biol Reprod*
783 100:398-408.

784 Sekulovski, N., A.E. Whorton, T. Tanaka, Y. Hirota, M. Shi, J.A. MacLean, J.R.L. de Mola, K. Groesch, P.
785 Diaz-Sylvester, and T. Wilson. 2020. Niclosamide suppresses macrophage-induced
786 inflammation in endometriosis. *Biol Reprod* 102:1011-1019.

787 Selection, W.E.C.o.t., U.o.E. Medicines, and W.H. Organization. 2014. The Selection and Use of Essential
788 Medicines: Report of the WHO Expert Committee, 2013 (including the 18th WHO Model List
789 of Essential Medicines and the 4th WHO Model List of Essential Medicines for Children). World
790 Health Organization,

791 Shi, M., N. Sekulovski, A.E. Whorton, J.A. MacLean, E. Greaves, and K. Hayashi. 2021. Efficacy of
792 niclosamide on the intra - abdominal inflammatory environment in endometriosis. *The FASEB
793 Journal* 35:e21584.

794 Smilde, A.K., H.A. Kiers, S. Bijlsma, C. Rubingh, and M. Van Erk. 2009. Matrix correlations for high-
795 dimensional data: the modified RV-coefficient. *Bioinformatics* 25:401-405.

796 Stuart, T., A. Butler, P. Hoffman, C. Hafemeister, E. Papalexi, W.M. Mauck III, Y. Hao, M. Stoeckius, P.
797 Smibert, and R. Satija. 2019. Comprehensive integration of single-cell data. *Cell* 177:1888-1902.
798 e1821.

799 Tao, H., Y. Zhang, X. Zeng, G.I. Shulman, and S. Jin. 2014. Niclosamide ethanalamine-induced mild
800 mitochondrial uncoupling improves diabetic symptoms in mice. *Nature medicine* 20:1263-
801 1269.

802 Thompson, S.M., Q.M. Phan, S. Winuthayanon, I.M. Driskell, and R.R. Driskell. 2021. Parallel single cell
803 multi-omics analysis of neonatal skin reveals transitional fibroblast states that restricts
804 differentiation into distinct fates. *J Invest Dermatol*

805 Wang, A.M., H.H. Ku, Y.C. Liang, Y.C. Chen, Y.M. Hwu, and T.S. Yeh. 2009. The autonomous notch signal
806 pathway is activated by baicalin and baicalein but is suppressed by niclosamide in K562 cells.
807 *J. Cell. Biochem.* 106:682-692.

808 Yona, S., K.-W. Kim, Y. Wolf, A. Mildner, D. Varol, M. Breker, D. Strauss-Ayali, S. Viukov, M. Guilliams,
809 and A. Misharin. 2013. Fate mapping reveals origins and dynamics of monocytes and tissue
810 macrophages under homeostasis. *Immunity* 38:79-91.

811 You, S., R. Li, D. Park, M. Xie, G.L. Sica, Y. Cao, Z.-Q. Xiao, and X. Deng. 2014. Disruption of STAT3 by
812 niclosamide reverses radioresistance of human lung cancer. *Mol. Cancer Ther.* 13:606-616.

813 Yu, G., L.-G. Wang, Y. Han, and Q.-Y. He. 2012. clusterProfiler: an R package for comparing biological
814 themes among gene clusters. *OMICS: J. Integrative Biol.* 16:284-287.

815 Yu, K., M.J. Gu, Y.J. Pyung, K.-D. Song, T.S. Park, S.H. Han, and C.-H. Yun. 2020. Characterization of splenic
816 MRC1 hi MHCII lo and MRC1 lo MHCII hi cells from the monocyte/macrophage lineage of White
817 Leghorn chickens. *Vet Res* 51:1-16.

818 Zeng, Z., B.G. Surewaard, C.H. Wong, C. Guettler, B. Petri, R. Burkhard, M. Wyss, H. Le Moual, R.
819 Devinney, and G.C. Thompson. 2018. Sex-hormone-driven innate antibodies protect females
820 and infants against EPEC infection. *Nat. Immunol.* 19:1100-1111.

821 Zhang, Y.-K., Z.-J. Huang, S. Liu, Y.-P. Liu, A.A. Song, and X.-J. Song. 2013. WNT signaling underlies the
822 pathogenesis of neuropathic pain in rodents. *The Journal of Clinical Investigation* 123:2268-
823 2286.

824 Zhao, L., N.C. Law, N.A. Gomez, J. Son, Y. Gao, X. Liu, J.M. de Avila, M.J. Zhu, and M. Du. 2021. Obesity
825 Impairs Embryonic Myogenesis by Enhancing BMP Signaling within the Dermomyotome.
826 *Advanced Science* 8:2102157.

827 Zhao, L., J.S. Son, B. Wang, Q. Tian, Y. Chen, X. Liu, J.M. de Avila, M.-J. Zhu, and M. Du. 2020. Retinoic
828 acid signalling in fibro/adipogenic progenitors robustly enhances muscle regeneration.
829 *EBioMedicine* 60:103020.

830 Zhou, J., B.S.M. Chern, P. Barton-Smith, J.W.L. Phoon, T.Y. Tan, V. Viardot-Foucault, C.W. Ku, H.H. Tan,
831 J.K.Y. Chan, and Y.H. Lee. 2020. Peritoneal fluid cytokines reveal new insights of endometriosis
832 subphenotypes. *Int. J. Mol. Sci.* 21:3515.

833 Zondervan, K.T., C.M. Becker, K. Koga, S.A. Missmer, R.N. Taylor, and P. Viganò. 2018. Endometriosis.
834 *Nature Reviews Disease Primers* 4:9.

835 Zondervan, K.T., C.M. Becker, and S.A. Missmer. 2020. Endometriosis. *New Engl J Med* 382:1244-1256.
836

837

838 **Figure Legends**

839 **Figure 1 Single-cell transcriptomic profiling of peritoneal immune cells. (A)**

840 Schematic of the experimental pipeline. (B) UMAP visualization of peritoneal
841 immune cells. (C) Ratios of each population in cell number. (D) VlnPlot of
842 characteristic gene expressions for macrophage subpopulations. Sham, sham control;
843 ELL, endometriosis-like lesions; ELL_N, niclosamide administration to ELL-induced
844 mouse; DC1, dendritic cells 1; SPMs, “small” peritoneal macrophages; IMS,
845 intermediate “small” macrophages; IML1, intermediate “large” macrophages subtype
846 1; IML2, intermediate “large” macrophages subtype 2; RLMs, resident “large”
847 macrophages; PMs, proliferating macrophages; B1a, B1a cells; B1b, B1b cells; B2,
848 B2 cells; GC-Bs, germinal-center B cells; PB-Bs, plasma blast B cells; Cd4+ Ts,
849 Cd4+ T cells; Cd8+ Ts, Cd8+ T cells; Cd4-/Cd8- Ts, Cd4-/Cd8- T cells; Blast Ts,
850 blast T cells; DC2, dendritic cells 2; MCs, Mast cells; NTPs, neutrophils.

851

852 **Figure 2 Niclosamide finely reverses transcriptomic changes caused by**

853 **endometriosis-like lesions (ELL) to peritoneal macrophages. (A)** Venn diagram
854 shows the overlaps of enriched GSEA terms of biological processes between those
855 enhanced in by ELL (ELL/sham) and those reduced by niclosamide (ELL_N/ELL).
856 (B) Similar to (A) but shows the overlaps between enriched terms of those down-
857 regulated in ELL (ELL/sham) and up-regulated by niclosamide (ELL_N/ELL). (C)
858 Enriched GSEA terms of biological processes that were reduced within the ELL_N
859 group compared to the sham group. (D) Representative GSEA terms that were
860 enhanced by ELL (ELL/sham) and were decreased by niclosamide (ELL_N/ELL). (E)
861 Representative GSEA terms that were inhibited by ELL (ELL/sham) and were
862 reversed by niclosamide (ELL_N/ELL).

863

864 **Figure 3 Niclosamide up-regulated genes with specific distributions within the**
865 **“small” peritoneal macrophage lineage.** (A) Venn diagram shows that overlaps of
866 genes that were enhanced by ELL (ELL/sham) but decreased by niclosamide
867 (ELL_N/ELL). (B) Overlaps of genes that were inhibited by ELL (ELL/sham) but
868 enhanced by niclosamide (ELL_N/ELL). (C) Vlnplot shows representative genes that
869 were enhanced by ELL but were reduced by niclosamide treatment (ELL_N). (D)
870 Verification of differential gene expression by RT-qPCR. $*p < 0.05$, $**p < 0.01$, $***p < 0.001$, mean \pm SEM, n = 6 per each group. (E) UMAP of computationally selected
871 macrophage populations and the distribution of genes within them.
872

873

874 **Figure 4 Reconstruction of a pseudo-temporal trajectory for the early**
875 **differentiation of recruited macrophages.** (A) UMAP shows selected cells of
876 recruited “small” macrophages (left) and a trajectory path built by Monocle 3 (right).
877 (B) Dynamic changes of genes along this trajectory path of differentiation. (C) GO
878 terms of biological processes that were enriched by perturbed genes affected by
879 virtual KO of *Rentla*. (D) Flow cytometer isolation and quantification of Ly6c+
880 recruited monocytes. (E) Flow cytometer results and quantification of CD206+ and
881 FR β + macrophages. $*p < 0.05$, $**p < 0.01$, mean \pm SEM, n = 5 per each group.

882

883 **Figure 5. Niclosamide downregulated genes with specific distributions within the**
884 **“large” peritoneal macrophage lineage.** (A) Vlnplot shows representative genes that
885 were reduced by ELL (ELL/sham) but were enhanced by niclosamide (ELL_N/ELL).
886 (B) Verification of differential gene expression by RT-qPCR. $*p < 0.05$, $**p < 0.01$,

887 *** $p < 0.001$, mean \pm SEM, n = 6 per each group . (C) UMAP of computationally
888 selected macrophage populations and the distribution of genes within them.

889

890 **Figure 6 Reconstruction of a pseudo-temporal trajectory for maturation of**
891 **intermediate “large” macrophages.** (A). UMAP shows selected cells of “large”
892 macrophages (left) and a trajectory path built by Monocle 3 (right). (B). Dynamic
893 changes of genes along this trajectory path of maturation and replenishment. (C). GO
894 terms of biological processes that were enriched by perturbed genes affected by
895 virtual KO of *Cfb*.

896

897 **Figure 7 Niclosamide preserves the population of embryo-derived resident**
898 **“large” peritoneal macrophages (RLMs).** (A) Vlnplot shows gene expression of
899 *Timd4* and *Apoc1*. (B) Feature plot shows the distribution of *Timd4* and *Apoc1*. (C)
900 Dynamic changes of genes along the trajectory path of maturation and replenishment
901 (D) GO terms of biological processes that were enriched by perturbed genes affected
902 by virtual KO of *Timd4*. (E) Flow cytometer isolation and quantification of TIM4+
903 resident macrophages.** $p < 0.01$, mean \pm SEM, n = 5 per each group.

904

905 **Figure 8 Niclosamide rescued the disrupted intercellular communications from**
906 **macrophages to B cells.** (A) Heatmap showing the interactions between
907 macrophages and B cells in terms of CCL signaling networks. (B) Heatmap showing
908 the interactions between macrophages and B cells in terms of CXCL signaling
909 networks. (C) Bubble plot showing all significant expressed ligand-receptor pairs
910 identified between three “large” macrophages (IML1, IML2, RLMs) and three
911 subtypes of B cells (B1a, B1b, B2). (D) Vlnplot showing the differential expressed

912 genes in macrophages. (E) Overlaps of GO biological processes in B cells that were
913 suppressed by ELL (ELL/sham) but enhanced by niclosamide (ELL_N/ELL). (F)
914 Overlaps of GO biological processes in B cells that were promoted by ELL
915 (ELL/sham) but suppressed by niclosamide (ELL_N/ELL). (G) Overlaps of GO
916 biological processes that were promoted by ELL by suppressed by niclosamide.

917 **Supplemental Figure Legends**

918 **Figure S1 Characteristics of immune cells at the single-cell level. (A)** Dot plot

919 showing one selected lineage-specific marker gene expression for each cluster. **(B)**

920 UMAP distribution of cell populations within three groups. **(C)** Characteristic

921 expression of marker genes for macrophage subpopulations.

922 Sham, sham control; ELL, endometriosis-like lesions; ELL_N, niclosamide

923 administration to ELL-induced mouse; DC1, dendritic cells 1; SPMs, “small”

924 peritoneal macrophages; IMS, intermediate “small” macrophages; IML1, intermediate

925 “large” macrophages subtype 1; IML2, intermediate “large” macrophages subtype 2;

926 RLMs, resident “large” macrophages; PMs, proliferating macrophages; B1a, B1a

927 cells; B1b, B1b cells; B2, B2 cells; GC-Bs, germinal-center B cells; PB-Bs, plasma

928 blast B cells; Cd4+ Ts, Cd4+ T cells; Cd8+ Ts, Cd8+ T cells; Cd4-/Cd8- Ts, Cd4-

929 /Cd8- T cells; Blast Ts, blast T cells; DC2, dendritic cells 2; MCs, Mast cells; NTPs,

930 neutrophils.

931

932 **Figure S2 Enriched GO terms of biological processes by the top 100 expressed**

933 **genes within each macrophage subpopulation to show their characteristic**

934 **profiles.**

935 DC1, dendritic cells 1; SPMs, “small” peritoneal macrophages; IMS, intermediate

936 “small” macrophages; IML1, intermediate “large” macrophages subtype 1; IML2,

937 intermediate “large” macrophages subtype 2; RLMs, resident “large” macrophages.

938

939 **Figure S3 Re-analysis of a single-cell transcriptomic dataset of peritoneal**

940 **macrophages in female mice in a normal physiological state from a public**

941 **resource.**

942 (A) UMAP visualization of macrophage populations. B) Gene markers used for
943 macrophage subpopulation clustering. (C) Feature plot showing the distribution of
944 genes. DC, dendritic cells; SPM, “small” peritoneal macrophages; IMS, intermediate
945 “small” macrophages; LPM1-4, intermediate “large” macrophages 1-4; PMs,
946 proliferating macrophages.

947

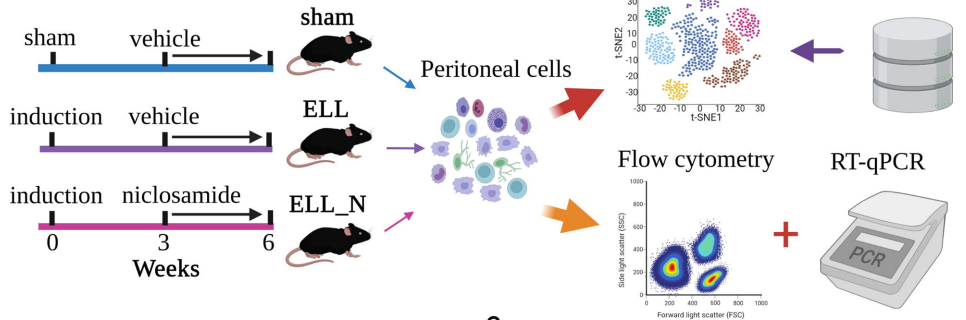
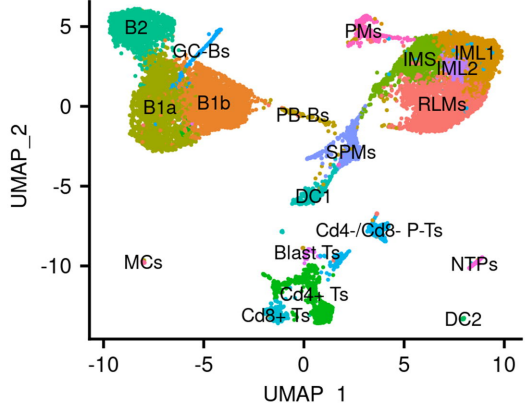
948 **Figure S4 Reconstruction of a trajectory path for the differentiation of recruited
949 macrophages (data from a public resource)**

950 (A) UMAP showing the selected cells (DC, SPM, and IMS) and the trajectory path
951 built within them. (B) Dynamic expression of genes along this trajectory path. DC,
952 dendritic cells; SPM, “small” peritoneal macrophages; IMS, intermediate “small”
953 macrophages.

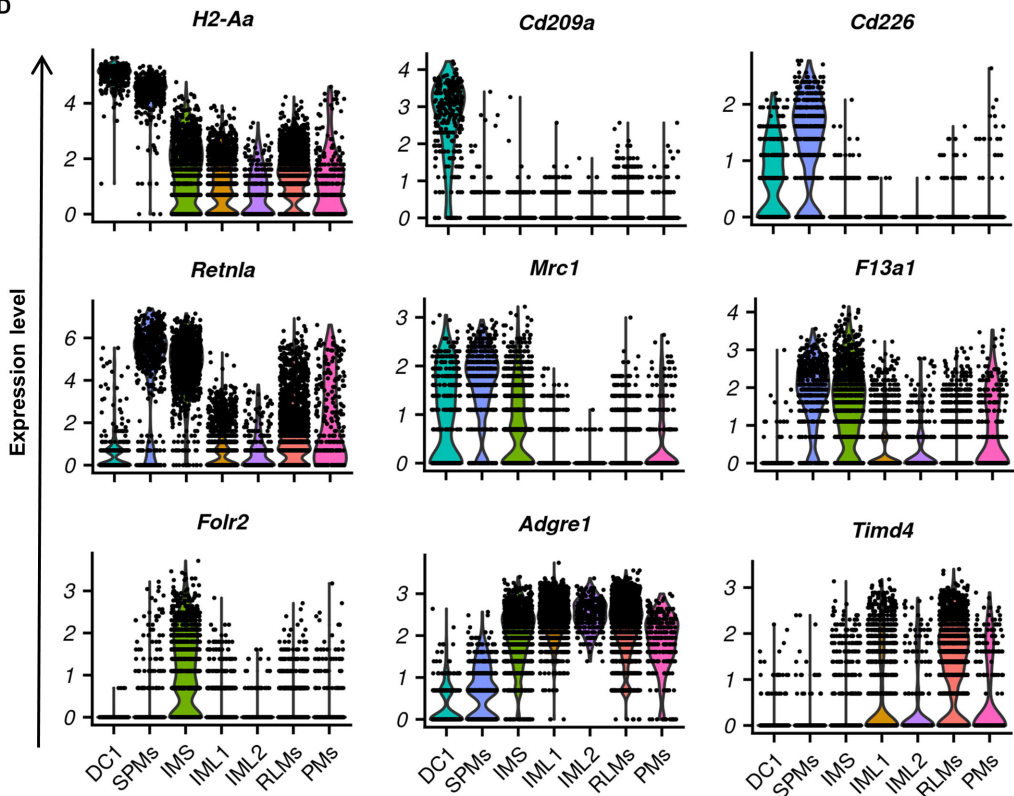
954

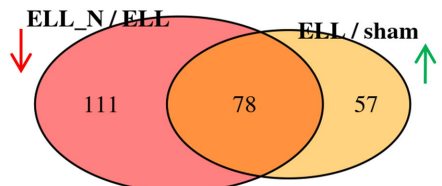
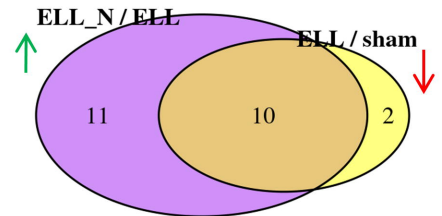
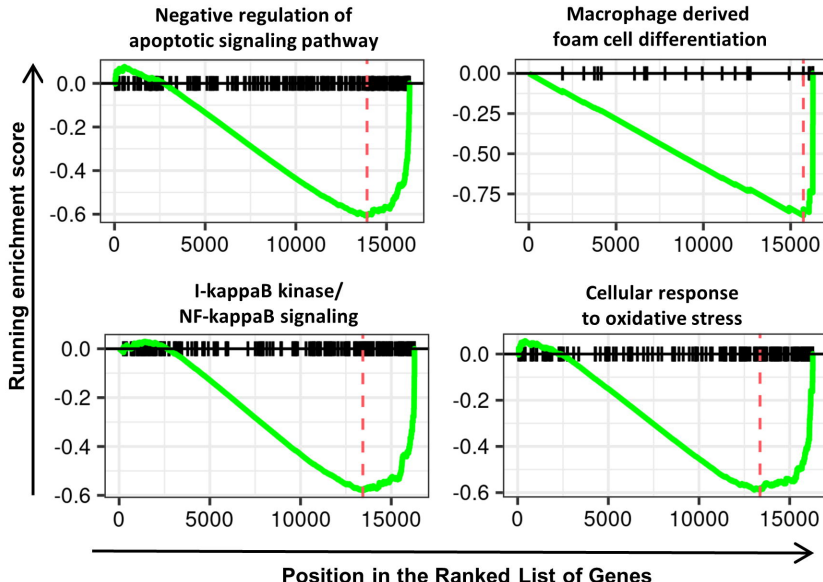
955 **Figure S5 Reconstruction of a trajectory path for “large” macrophages**

956 (A) UMAP showing the selected cells (LPM1-4) and the trajectory path built within
957 them. (B) Dynamic expression of genes along this trajectory path. LPM1-4,
958 intermediate “large” macrophages 1-4.

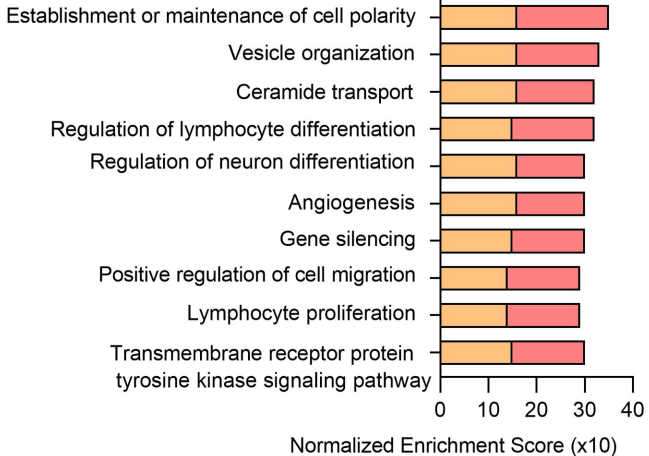
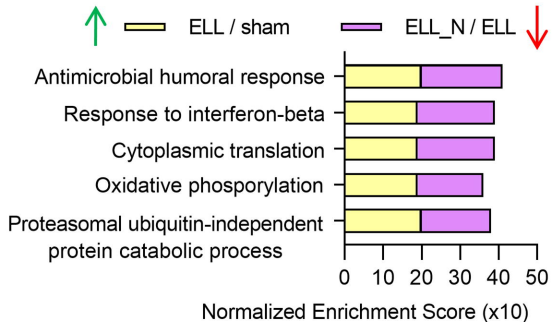
A**B****C**

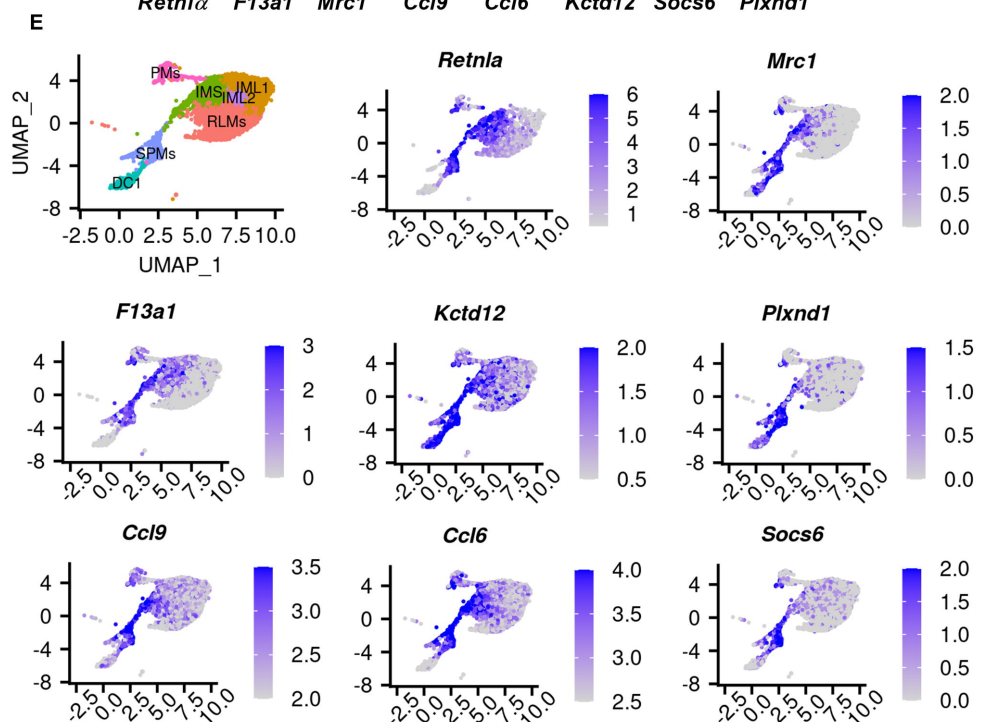
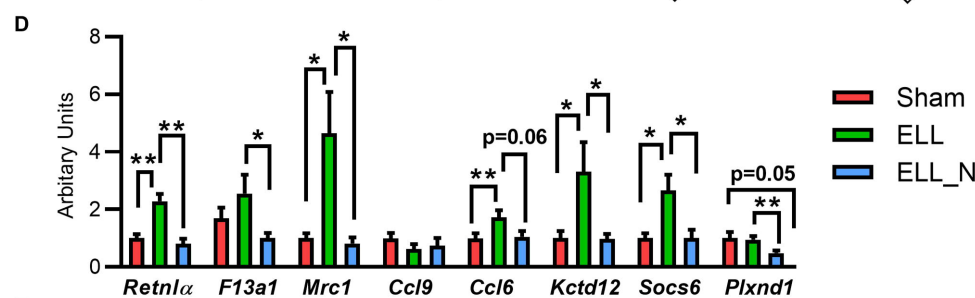
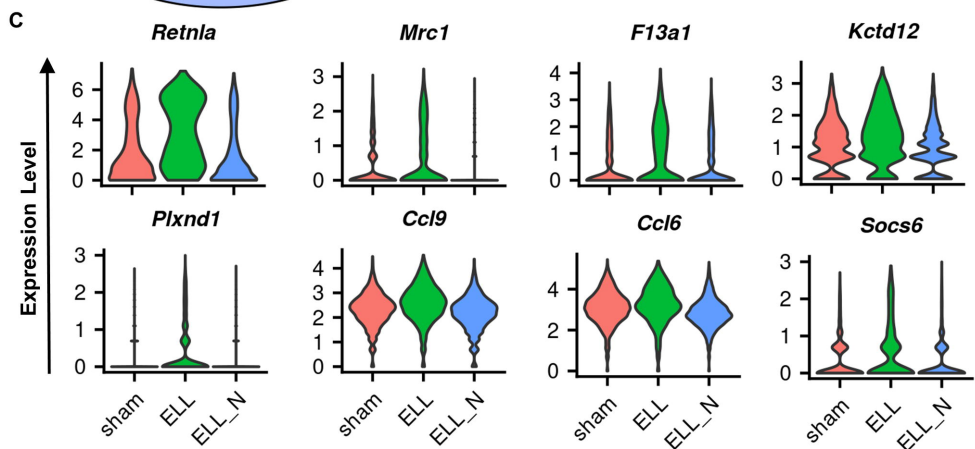
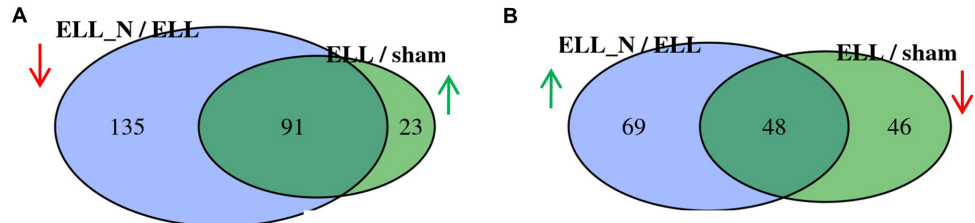
Macrophages	B cells	T cells & others
DC1 (2.1%)	B2 (10%)	Cd4+ Ts (5.1%)
SPMs (3.5%)	B1a (16%)	Cd8+ Ts (1.6%)
IMS (7.6%)	B1b (18%)	Cd4-/Cd8- Ts (2.4%)
IML1 (11%)	GC-Bs (0.8%)	Blast-Ts (0.29%)
IML2 (1.9%)	PB-Bs (1.3%)	DC2 (0.22%)
RLMs (15%)		MCs (0.17%)
PMs (1.9%)		NTPs (0.54%)

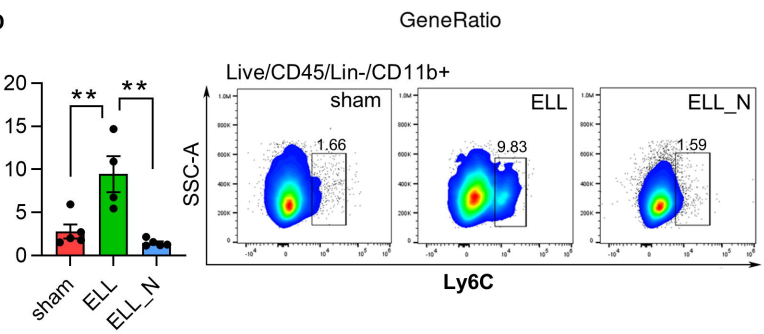
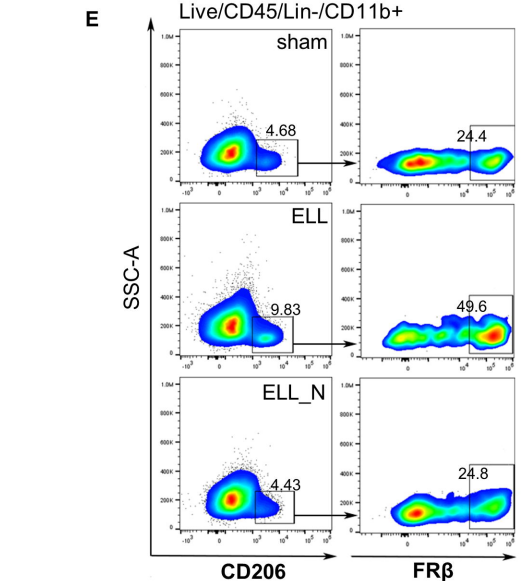
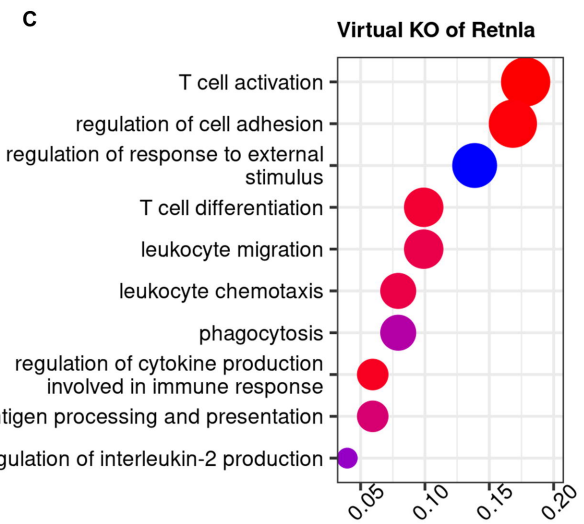
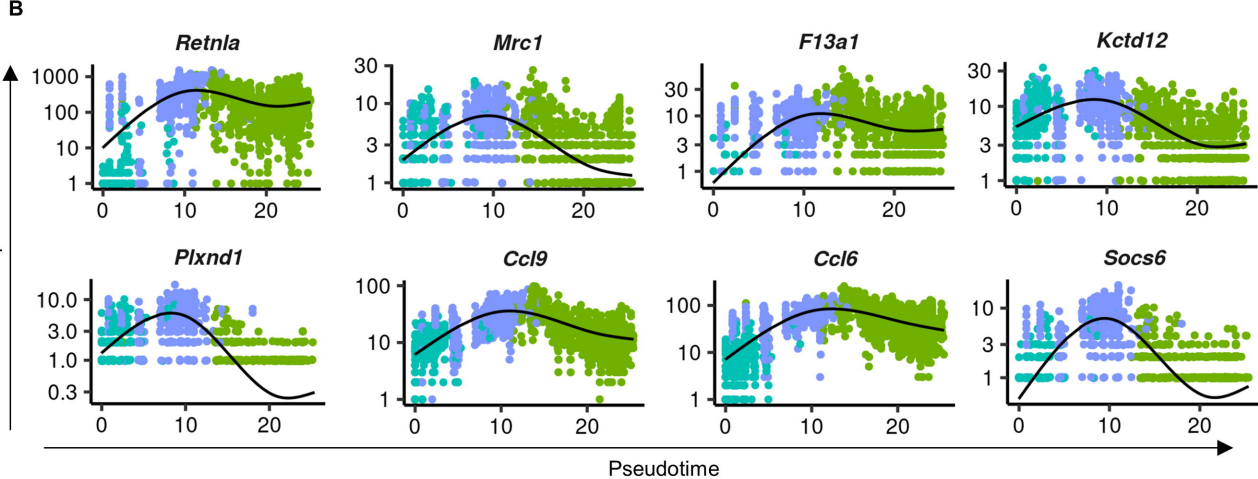
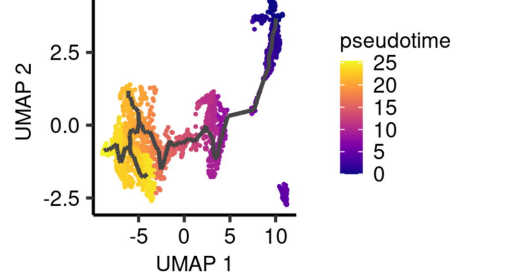
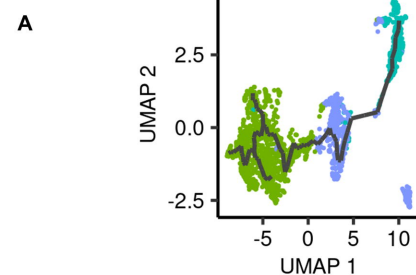
D

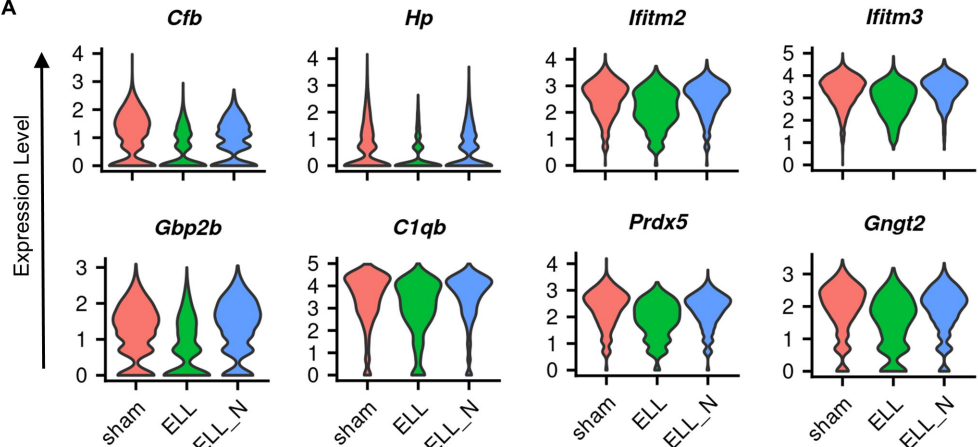
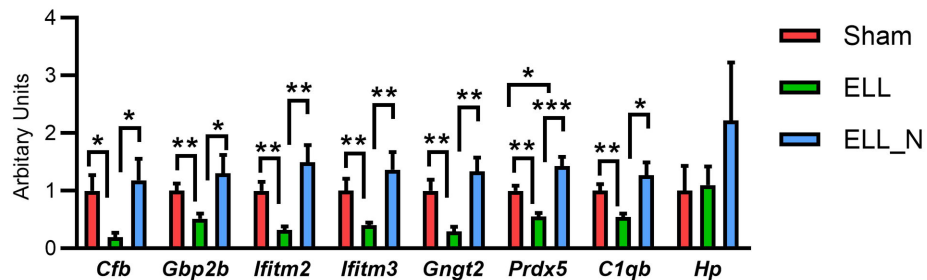
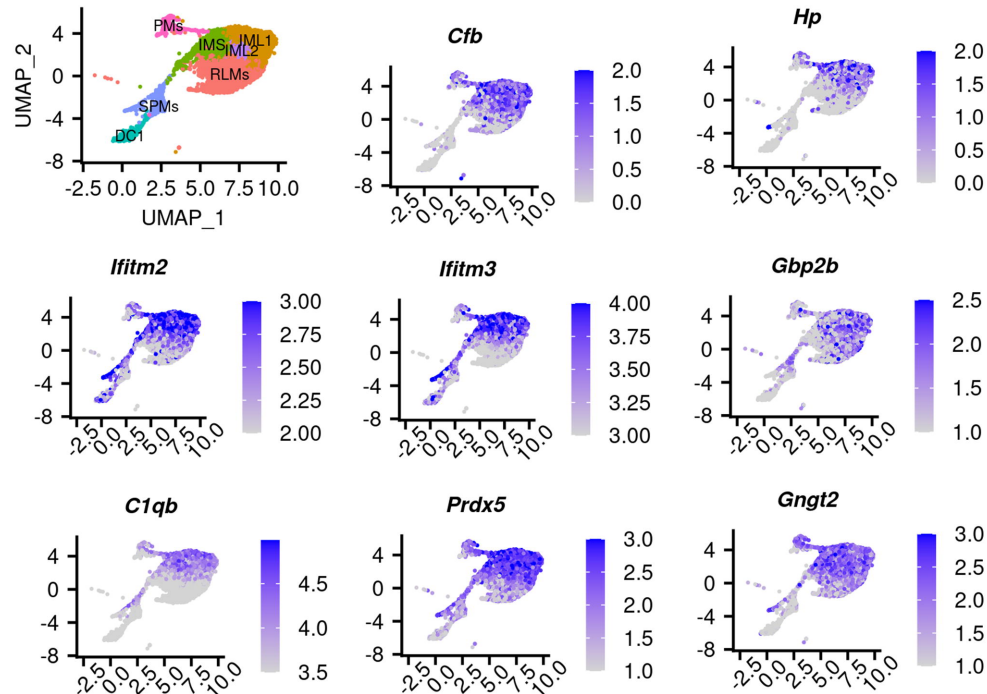
A**B****C****D**

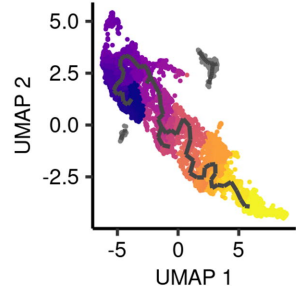
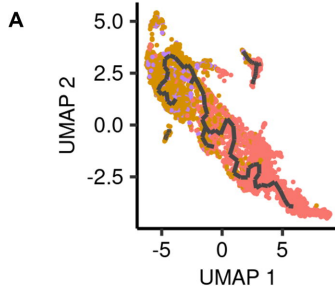
↓ ELL / sham ↑ ELL_N / ELL

**E**

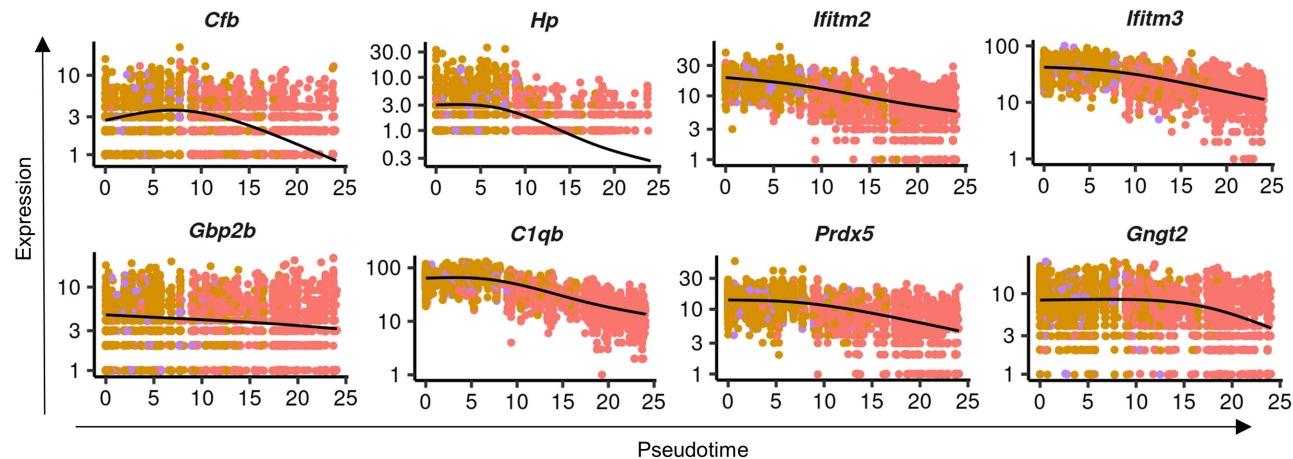




A**B****C**



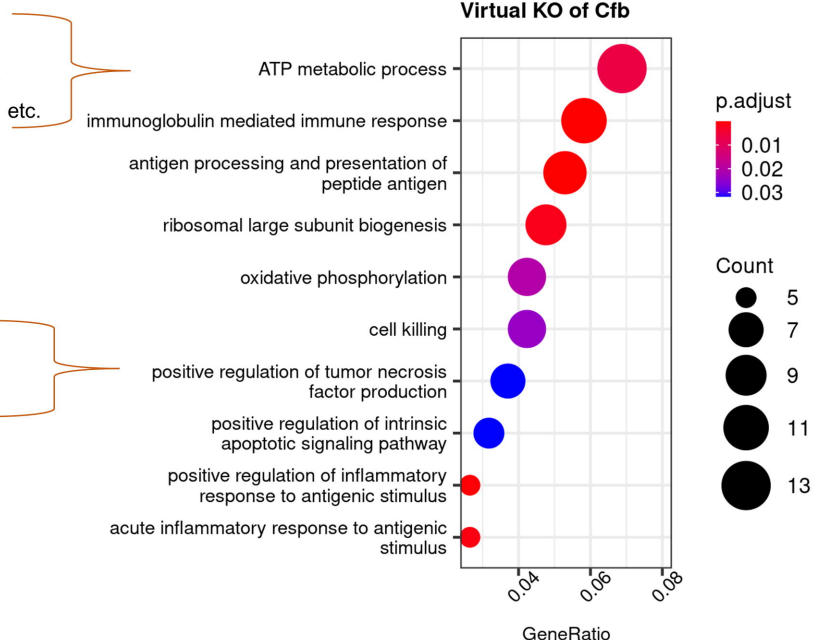
B

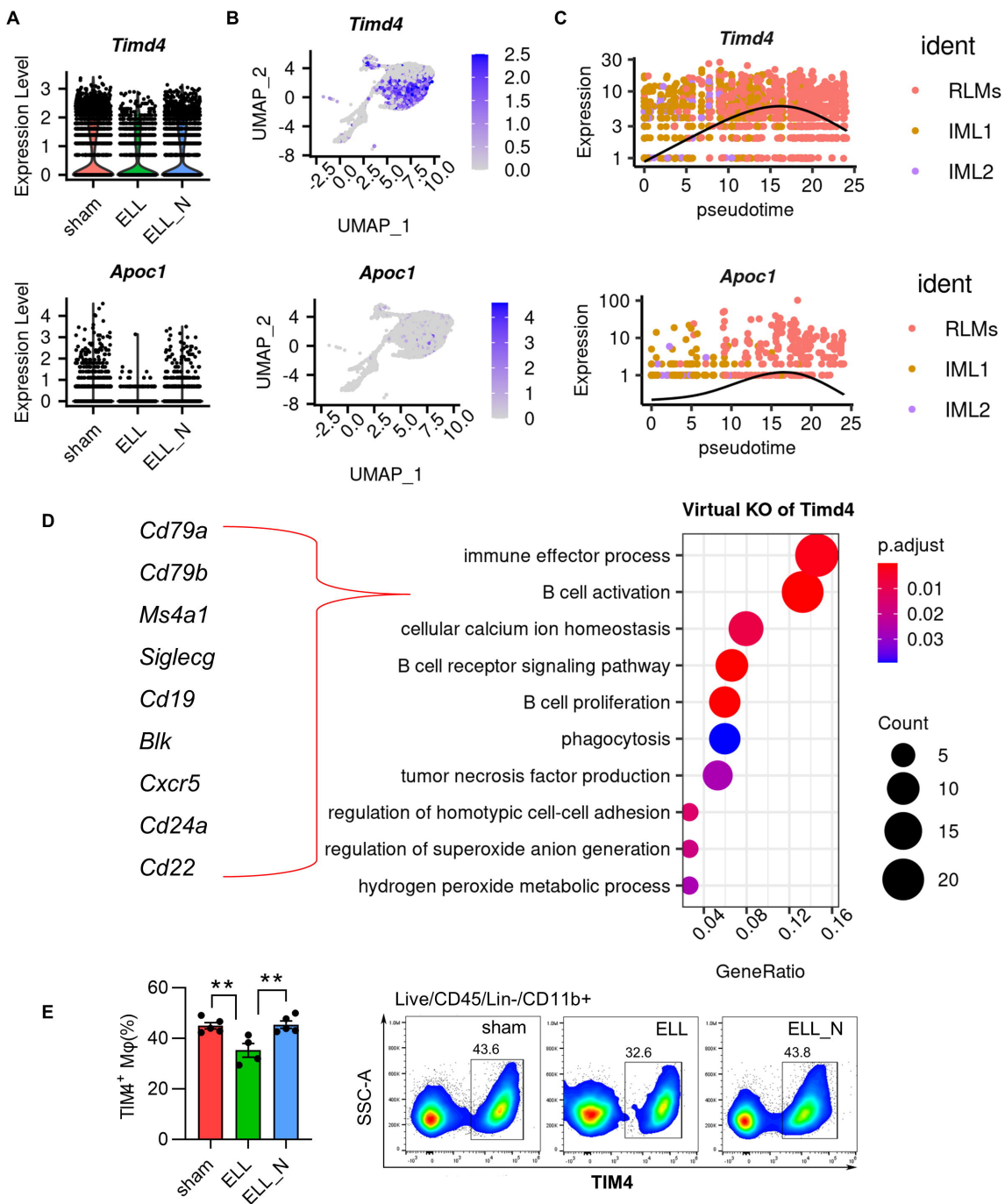


C

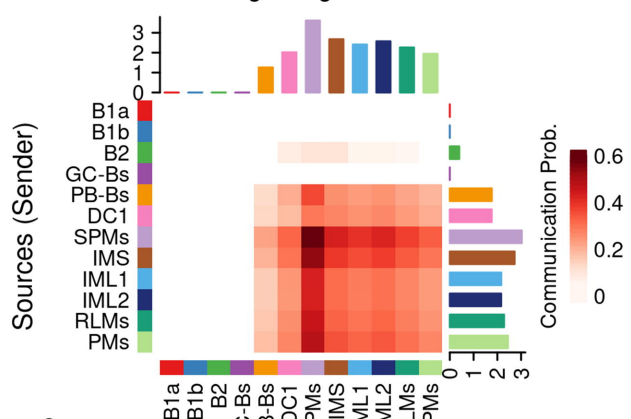
Nupr1, Eno1, Park7, Cox5b, Tspo, Atp5c1, Atp5b, Atp5d, Uqcrb, Ndufs8, Khk, Gapdh, etc.

Cd14, Cyba, Tyrobp, Fcgr1g, Fcgr3, Pycard, H2-T23, etc.

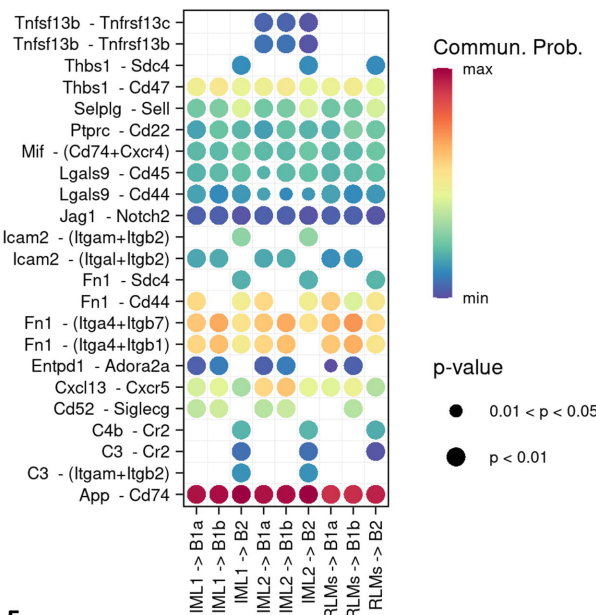




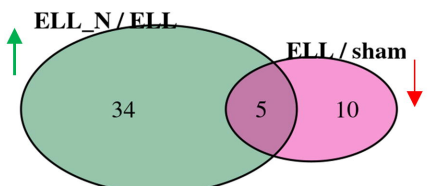
A CCL signaling network



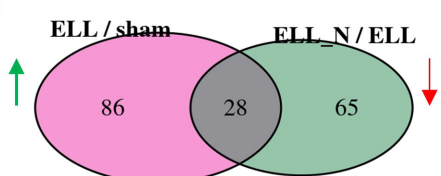
C



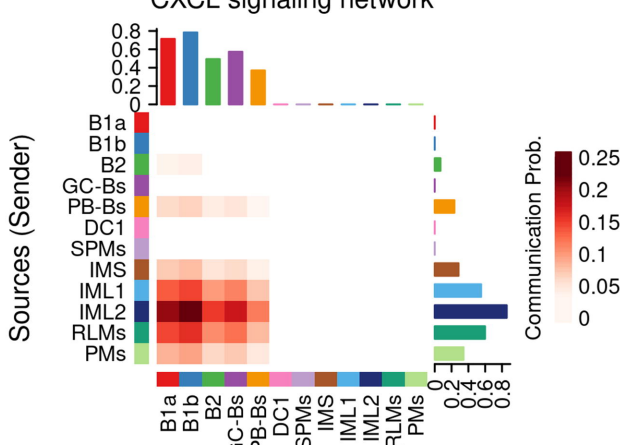
E



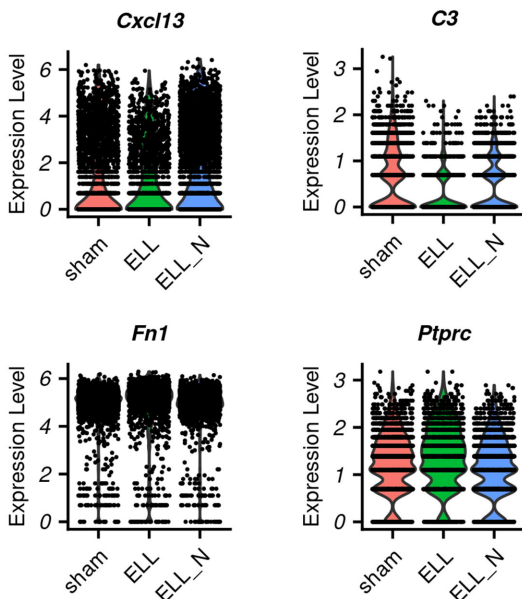
F



B CXCL signaling network



D



G

